

UC San Diego

UC San Diego Electronic Theses and Dissertations

Title

Spin dynamics in nanomagnetic structures

Permalink

<https://escholarship.org/uc/item/9vc165b9>

Author

Zhuang, Shihao

Publication Date

2018

Peer reviewed|Thesis/dissertation

UNIVERSITY OF CALIFORNIA SAN DIEGO

Spin dynamics in nanomagnetic structures

A Thesis submitted in partial satisfaction of the requirements
for the degree Master of Science

in

Materials Science and Engineering

by

Shihao Zhuang

Committee in charge:

Vitaliy Lomakin, Chair
Prabhakar Bandaru
Vlado Lubarda

2018

Copyright

Shihao Zhuang, 2018

All rights reserved.

The Thesis of Shihao Zhuang is approved, and it is acceptable in quality and form for publication on microfilm and electronically:

Chair

University of California San Diego

2018

TABLE OF CONTENTS

Signature Page	iii
Table of Contents	iv
List of Figures.....	v
List of Tables	vii
Abstract of the Thesis	viii
Chapter 1 Introduction.....	1
Chapter 2 Micromagnetic modeling.....	3
2.1 Finite element modeling	4
2.2 Landau-Lifshitz-Gilbert equation	5
2.3 Dominant interactions in micromagnetics	7
2.3.1 Zeeman interaction.....	7
2.3.2 Magnetostatic interaction	8
2.3.3 Magnetocrystalline anisotropy	11
2.3.4 Exchange interaction.....	13
2.4 Domain walls	14
Chapter 3 Spin dynamics in nanomagnetic structures.....	18
3.1 Spin polarization	19
3.2 Spin valve and spin transfer torque.....	21
3.3 Spin transfer torque in micromagnetics	24
3.4 Spin diffusion model.....	26
3.4.1 Continuous formulation	26
3.4.2 Discrete node-based formulation	28
3.4.3 Discrete element-based formulation — weak formulation	32
3.4.4 Spin diffusion model coupled with the LLG equation.....	34
3.5 Numerical experiments	35
3.5.1 Multi-layered structure.....	35
3.5.2 Néel domain wall	40
3.5.3 Magnetization dynamics with STT effect.....	42
Chapter 4 Conclusion	45
Bibliography	47

LIST OF FIGURES

Figure 2.1: Mesh of and elliptical cylinder and a typical tetrahedral element.	5
Figure 2.2: Precession of magnetic moment about effective magnetic field.	6
Figure 2.3: Magnetic dipole field.....	8
Figure 2.4: Calculation of demagnetizing field by summing up dipole fields and by potential approach.....	9
Figure 2.5: Hexagonal close packed crystal structure with uniaxial anisotropy and body centered cubic crystal structure with cubic anisotropy.	12
Figure 2.6: Ferromagnetism and antiferromagnetism.....	14
Figure 2.7: Hypothetical and real domain wall structure.....	15
Figure 2.8: Bloch domain wall and Neel domain wall.	16
Figure 2.9: Variation of the angle between magnetization and the easy axis with respect to the position in the domain wall.	17
Figure 3.1: Schematic representing the density of states function in 3d and 4s energy band of nickel.	20
Figure 3.2: A normal metal / ferromagnet / normal metal junction.	22
Figure 3.3: A normal metal / ferromagnet / normal metal / ferromagnet / normal metal spin valve.	23
Figure 3.4: Tetrahedral finite element mesh for Slonczewski model.	24
Figure 3.5: Tetrahedron l with four vertices q, r, s, t, appearing in (3.15) to (3.17).....	29
Figure 3.6: Schematic representation of the continuity of the spin current, appearing in (3.21).	31
Figure 3.7: A 1×1×28 nm multi-layer spin valve	35
Figure 3.8: Comparison between node-based method solution and Galerkin method weak solution.....	37
Figure 3.9: Variation of the spin accumulation in the valve in 10 fs.....	38
Figure 3.10: Evolution of the spatially averaged spin accumulation in 175 fs.	39
Figure 3.11: The spin accumulation under equilibrium in the multi-layer spin valve.....	39
Figure 3.12: Néel domain wall in a 600×100×1 nm thin bar.	40
Figure 3.13: Spin accumulation generated by the Neel wall in the thin bar	40

Figure 3.14: Comparison between the magnitude of the spin transfer torque calculated by Zhang & Li model and spin diffusion model.....	42
Figure 3.15: MRAM – stacked-layer structure.....	43
Figure 3.16: Evolution of the magnetization in the free layer.....	44

LIST OF TABLES

Table 3.1: Timing statistics – solution in multi-layered structure by node-based method.....	36
Table 3.2: Timing statistics – solution in multi-layered structure by element-based method..	36
Table 3.3: Timing statistics – solution in Néel wall case by node-based method.....	41
Table 3.4: Timing statistics – solution in Néel wall case by element-based method.....	41

ABSTRACT OF THE THESIS

Spin dynamics in nanomagnetic structures

by

Shihao Zhuang

Master of Science in Materials Science and Engineering

University of California San Diego, 2018

Professor Vitaliy Lomakin, Chair

The development of the spintronic-based data storage devices such as spin transfer torque magnetoresistive random access memory (STT-MRAM) is being driven by the surging data consumption and demand for faster data processing. The advantages of nonvolatility, higher data processing speed, lower power consumption and scalability hold the promise of the popularity of STT-MRAM in the future, of which spin transfer torque (STT) effect is the key. This thesis develops a spin diffusion model to study the spin dynamics in nanomagnetic structures and the corresponding STT effect acting on local magnetic moments. Chapter 2 provides an introduction to micromagnetic modeling, dominant magnetic interactions, and

domain walls. Chapter 3 presents spin diffusion model, in which two approaches are discussed for handling the boundary conditions and we demonstrate their good performance in solving spin diffusion equation in finite element models. Chapter 3 also shows solutions for the spin accumulation in multi-layered magnetic structures at equilibrium and in dynamics. It also studies the case of spin transfer torque in magnetic nanostructures with the Néel wall, comparing it to the simplified Zhang & Li model. At the end of the chapter 3 we simulate the magnetization dynamics under STT effect using the FastMag micromagnetic simulation software coupled with the spin diffusion model.

Chapter 1

Introduction

In twentieth century the mainstream electronic devices were based on the electron charge. While it was known for long that electrons possess angular momentum and the associated magnetic moments, no practical application made use of this property until recently. The technology that exploits electron spins and its influences on electrical conduction and magnetic states emerged in late twentieth century when the spin polarized current injection from a ferromagnetic material to a normal metal was observed by Mark Johnson and R. H. Silsbee [1], and the giant magnetoresistance was discovered by Albert Fert [2] and Peter Grünberg in 1988 [3]. Nowadays, the development of spintronics based devices is envisioned by scientific community and industry. Among them, data storage devices such as magnetoresistive random access memory (MRAM), spin transfer torque MRAM (STT-MRAM) and domain wall based racetrack memory, are the main market of spin electronics due to the surging demand for storage capacity and speed following the increasing data consumption. The advantages of nonvolatility, higher data processing speed, lower power consumption, and scalability hold the promise of popularity of spintronics based data storage devices [4, 5].

Numerical simulations provide a great insight and prediction of experiment, which improves efficiency and reduces the cost of research and design. The FastMag code developed

at UCSD is such a computational framework, which contains several modules that make it fit to the simulation of many types of physical models and devices in nanomagnetism. The computations are based on micromagnetic modeling and take advantage of efficient algorithms, parallel computing, and high-performance Graphics Processing Units (GPUs) in order to efficiently solve magnetization dynamics in complex magnetic systems.

This thesis presents how spin dynamics in nanomagnetic structures can be solved in a finite element model and coupled with micromagnetic models to simulate spin transfer torque effects. Chapter 2 reviews the basic knowledge of micromagnetic modeling in terms of the expressions of the variables and the most important magnetic interactions in a finite element scheme. The brief introduction of domain wall is also present. Chapter 3 reiterates some concepts and phenomena in spintronics related to this work and introduces Slonczewski's model, Zhang & Li's model, and spin diffusion model. Different computational methods of solving spin diffusion equation are compared and the capability of the spin diffusion model to study spin dynamics and spin transfer torque effect is demonstrated. The model has advantages over the models of Slonczewski and Zhang & Li.

Chapter 2

Micromagnetic modeling

All interactions between magnetic moments can be in principle described by atomistic formulations taking atomistic and electronic consideration. Micromagnetics is a discipline that deals with magnetic phenomena at mesoscale, i.e. the length scale large enough for materials structure to be thought of as continuous but small enough to solve magnetic behaviors such as domain wall formation, motion, and magnetization dynamics. Micromagnetics was introduced in W. F. Brown's work [6] through treatments of magnetic interaction energies, in which magnetic moments density and materials parameters were assumed to be continuous. While the magnetization configuration at equilibrium can be found by solving Brown's equation, the Landau-Lifshitz-Gilbert (LLG) equation [7, 8] is typically used to describe the magnetization dynamics. The magnetization dynamics in the LLG equation is driven by the effective field, which describes various physical interactions. This chapter introduces major interactions in micromagnetics and magnetic domain wall relevant to this work.

2.1 Finite element modeling

The first step in solving magnetization dynamics in a part of material or a device is to discretize all volumes of the system into finite elements. In our case, the systems to be studied are discretized into tetrahedrons, each node in the mesh is linked to the neighboring tetrahedral elements and their nodes. A magnetization vector \mathbf{M} is assigned to each mesh node (tetrahedron vertex) (figure 2.1). To comply with continuum approximation of micromagnetics, \mathbf{M} must be continuous throughout the system, thus, we define $\mathbf{M}^l(\mathbf{r})$ in each tetrahedron l , and represent it using

$$\mathbf{M}^l(\mathbf{r}) = \sum_{k=1}^4 \mathbf{M}_k^l \xi_k^l(\mathbf{r}), \quad (2.1)$$

where \mathbf{M}_k^l is the magnetization vector at each of the four vertices of the tetrahedron l , and $\xi_k^l(\mathbf{r})$ is a linear basis function, which is equal to unity at vertex k and linearly goes down to zero toward the opposite face. The relation between neighboring nodes is mathematically described by linear basis function, which is the foundation of the expressions of variables, material parameters and mathematical operations such as gradient and Laplacian matrices in discretized scheme.

Generally, the distance between the adjacent nodes ranges from less than a nanometer to tens of nanometers, which depends on the size of specific system and is limited by critical scales, the typical one is critical length induced by exchange interaction, defined as $l_{ex} = \sqrt{A_{ex}/K}$, where A_{ex} is exchange stiffness constant and K is anisotropy energy density.

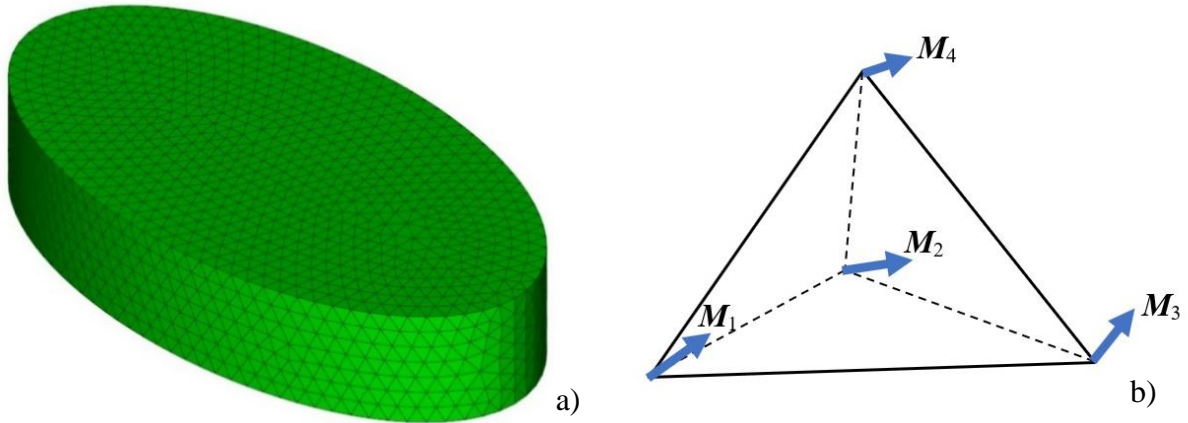


Figure 2.1: a) A mesh of an elliptical cylinder divided into tetrahedrons in finite element model. b) A typical tetrahedral element with four unit magnetization vectors prescribed at each vertex. The unit magnetization is expressed throughout the system using linear basis function.

2.2 Landau-Lifshitz-Gilbert equation

The Landau-Lifshitz-Gilbert equation is written as

$$\frac{d\mathbf{M}}{dt} = -\gamma\mathbf{M} \times \mathbf{H}_{eff} + \alpha\mathbf{M} \times \frac{d\mathbf{M}}{dt}, \quad (2.2)$$

where γ is the gyromagnetic ratio, α is the damping constant, \mathbf{M} is the magnetization, and \mathbf{H}_{eff} is the effective magnetic field. Two driving forces are taken into consideration in this equation: the first term on the right side of (2.2) represents the total torque applied by \mathbf{H}_{eff} and it leads to a precessional motion of magnetic moment about the effective magnetic field. The second term represents the damping during the precession due to loss of energy, with most of the lost energy transferred to the lattice in the form of heat [9] (figure 2.2).

However, the derivative terms with respect to \mathbf{M} are present on both sides of the equation, that is, the LLG equation in this form is implicit. The equation can be cast into an

explicit form by replacing $d\mathbf{M}/dt$ in the right-hand side with the entire right-hand side of the LLG equation:

$$\frac{d\mathbf{M}}{dt} = -\gamma\mathbf{M} \times \mathbf{H}_{eff} + \alpha\mathbf{M} \times \left(-\gamma\mathbf{M} \times \mathbf{H}_{eff} + \alpha\mathbf{M} \times \frac{d\mathbf{M}}{dt} \right), \quad (2.3)$$

It can be shown that

$$\mathbf{M} \times \mathbf{M} \times \frac{d\mathbf{M}}{dt} = -\frac{d\mathbf{M}}{dt}, \quad (2.4)$$

which leads to the LLG equation in the explicit form:

$$\frac{d\mathbf{M}}{dt} = -\frac{\gamma}{1+\alpha^2}\mathbf{M} \times \mathbf{H}_{eff} - \frac{\alpha\gamma}{1+\alpha^2}\mathbf{M} \times \mathbf{M} \times \mathbf{H}_{eff} \quad (2.5)$$

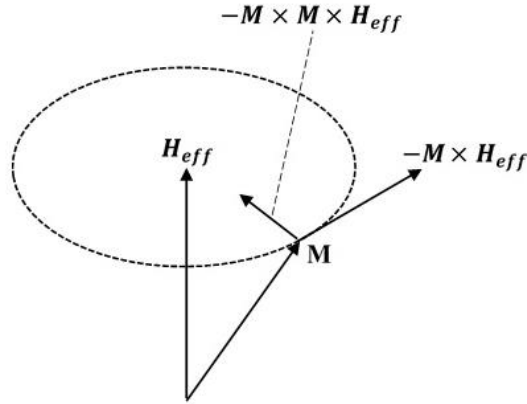


Figure 2.2: Precession of magnetic moment about effective magnetic field as axis. Damping term favors the magnetic moment in precession to align with the effective field.

In this work, an additional term representing spin transfer torque should be added to the LLG equation to describe the interaction between magnetic moments and spin accumulation. Spin polarized current, spin accumulation and spin transfer torque are introduced in more detail in chapter 3.

2.3 Dominant interactions in micromagnetics

The effective field \mathbf{H}_{eff} in equation (2.2) is the sum of the magnetic fields exerted on the magnetic moments by various interactions. There are many kinds of interactions that can be encountered in micromagnetics, however, compared to those dominant interactions that occur in most of situations, the rest of them are relatively negligible except under special situations [10, 11, 12, 13]. To speed up computation and save memory, generally, we only take into account the most dominant interactions: the Zeeman interaction, the magnetostatic interaction, the magnetocrystalline anisotropy, and the exchange interaction.

The corresponding fields can be derived through the derivative of their potential energy densities with respect to the magnetization:

$$\mathbf{H} = -\frac{\partial E}{\partial \mathbf{M}}. \quad (2.6)$$

2.3.1 Zeeman interaction

The Zeeman interaction is the one acted by externally applied magnetic fields \mathbf{H}_{app} and the associated potential energy, Zeeman energy, on magnetization \mathbf{M} is written as (in CGS system of units):

$$\mathbf{E}_z = -\int_V \mathbf{M} \cdot \mathbf{H}_{app} d^3\mathbf{r} \quad (2.7)$$

The Zeeman energy has its minimum when \mathbf{M} and \mathbf{H}_{app} are oriented in the same direction, meaning that the Zeeman interaction favors to align the magnetization parallel to the externally applied field.

Generally, \mathbf{H}_{app} is a variable input by users and added to the effective field \mathbf{H}_{eff} directly.

2.3.2 Magnetostatic interaction

Intrinsic magnetic moments are mainly contributed by electronic spin and its orbital motion around the nucleus [14], the field generated by one magnetic moment has the same form as that of electric dipole with the associated magnetic dipole field (figure 2.3) expressed as:

$$\mathbf{H}_{ms} = \frac{1}{4\pi} \left(\frac{3(\mathbf{M} \cdot \mathbf{r})\mathbf{r}}{r^5} - \frac{\mathbf{M}}{r^3} \right). \quad (2.8)$$

where \mathbf{M} is magnetization and r is the distance from the dipole to the considered point.

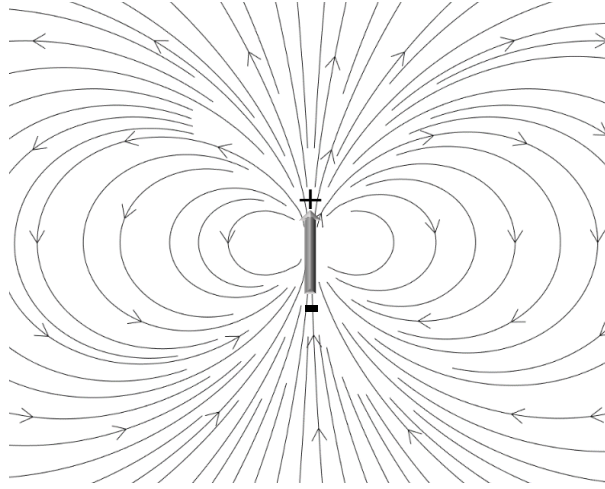


Figure 2.3: The magnetic field generated by a magnetic dipole moment.

Each dipole in the magnetic system generates such a magnetic field in the entire space, so each magnetic moment interacts with each other ones through its dipole field, in this case, also called magnetostatic field or demagnetizing field, and the interaction is called the

magnetostatic interaction. The field can be regarded as externally applied field whose source is inside the system, so the magnetostatic potential energy can be written as:

$$\mathbf{E}_{ms} = -\frac{1}{2} \int_V \mathbf{M} \cdot \mathbf{H}_{ms} d^3\mathbf{r}, \quad (2.9)$$

or in the discretized form:

$$\mathbf{E}_{ms} = -\frac{1}{2} \sum_{i=0}^N \sum_{j=0, j \neq i}^N V_i \mathbf{M}_i \mathbf{H}_{ms,j|i} \quad (2.10)$$

where N is the number of the vertices in the system of tetrahedrons and V_i is effective volume of the mesh node.

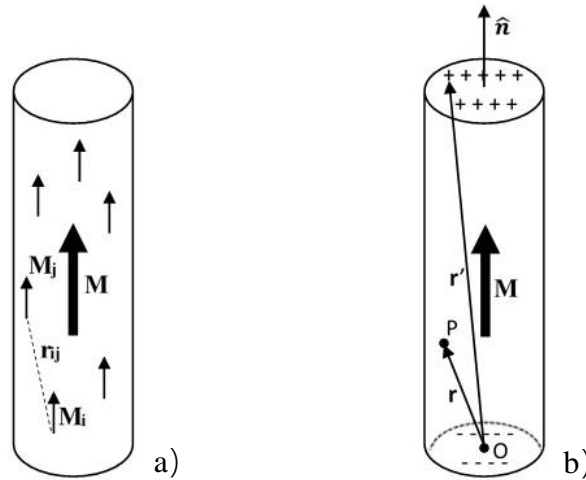


Figure 2.4: a) Calculate demagnetizing field by integrating or summing up all dipole fields over the entire system. b) Calculate demagnetizing field using potential approach, in which positive and negative magnetic charges are distributed on the surface of the system.

However, the approach is computationally expensive for numerical computation, because the magnetic system is composed of a large number of magnetic moments and we need to calculate each pair of magnetic moments in the system, which can significantly slow down

the simulations. To directly calculate the demagnetizing field, we can use the potential approach (figure 2.4 b) that replace the magnetic dipoles by an assumed distribution of magnetic charge:

$$\mathbf{H}_{ms} = -\nabla \int_V \frac{-\nabla \cdot \mathbf{M}'}{|\mathbf{r} - \mathbf{r}'|} d^3\mathbf{r}' - \nabla \oint_S \frac{\hat{\mathbf{n}} \cdot \mathbf{M}'}{|\mathbf{r} - \mathbf{r}'|} d^2\mathbf{r}'. \quad (2.11)$$

Better methods can be applied to the systems whose magnetization within a part of volume is uniform. In these cases, the positive and negative magnetic charges cancel out inside the volume and they only separately appear at the surfaces, generating a demagnetizing field, which can be computed using the demagnetizing tensor [15] The relation between \mathbf{H}_{ms} and \mathbf{M} can be expressed as:

$$\mathbf{H}_{ms,i} = -N_{ij}\mathbf{M}_j \quad (i, j = x, y, z), \quad (2.12)$$

where N_{ij} is the demagnetizing tensor, which is generally a 3×3 matrix, whose diagonal elements N_{xx}, N_{yy}, N_{zz} are known as demagnetizing factors and only two of them are independent because the demagnetizing tensor has unit trace:

$$N_{xx} + N_{yy} + N_{zz} = 1. \quad (2.13)$$

In the case in which the system has one or more axis or plane of symmetry, the non-diagonal elements $N_{ij, i \neq j} = 0$. For example, there is no preferential orientation of the magnetization in a magnetic sphere, so the only non-zero elements of the demagnetizing tensor are $N_{xx} = N_{yy} = N_{zz} = \frac{1}{3}$. In the case of a long magnetic needle, the N_{ii} for magnetization directing perpendicular to the axis is 0.5. As for a magnetic thin film, there is only one non-zero element which represents the magnetization perpendicular to the plane.

However, in many general cases without uniform magnetization configuration, demagnetizing field cannot be computed accurately using demagnetizing factors, so the field at

each point has to be computed directly through summing up all magnetic dipole fields (equation 2.8) generated by other magnetic moments (figure 2.4 a). In micromagnetic simulations, each node represents a magnetic moment and the coordinates of all nodes are known in advance, so we can precompute the demagnetizing tensor T_{ij} for each pair of nodes (i, j) , based on distance vector \mathbf{r}_{ij} between nodes i and j to save simulation time. The tensor for pair (i, j) is written as:

$$T_{ij} = \frac{1}{4\pi|\mathbf{r}_{ij}|^3} \begin{bmatrix} 3r_{x,ij}^2 - 1 & 3r_{x,ij}r_{y,ij} & 3r_{x,ij}r_{z,ij} \\ 3r_{y,ij}r_{x,ij} & 3r_{y,ij}^2 - 1 & 3r_{y,ij}r_{z,ij} \\ 3r_{z,ij}r_{x,ij} & 3r_{z,ij}r_{y,ij} & 3r_{z,ij}^2 - 1 \end{bmatrix} \quad (2.14)$$

and the demagnetizing field exerted on node i by the magnetic moment on node j is:

$$\mathbf{H}_{demag,j \rightarrow i} = T_{ij} \mathbf{M}_j \quad (2.15)$$

The total demagnetizing field applied on the node i is then the sum of $\mathbf{H}_{demag,j \rightarrow i}$:

$$\mathbf{H}_{demag,i} = \sum_{j=0, j \neq i}^N T_{ij} \mathbf{M}_j \quad (2.16)$$

where N is the number of mesh nodes.

2.3.3 Magnetocrystalline anisotropy

Magnetocrystalline anisotropy means that one or more axes leading to preferential magnetization orientation lie in ferromagnetic or antiferromagnetic sample. The axes in preferential direction are called easy axes, and those that are disfavored by magnetocrystalline anisotropy are called hard axes. Possessing strong easy axes is a prerequisite for hard magnets and near zero anisotropy for soft magnets [16]. Magnetocrystalline anisotropy is an intrinsic material property that indicates the crystal symmetry and it originates from crystal-field interaction, spin-orbit interaction and interatomic dipoles interaction [17].

Materials with different lattice structure have different numbers and directions of anisotropy easy axes [18]. The most common type is the uniaxial anisotropy for which there exists one easy axis and thus two preferential orientation of magnetization (figure 2.5 a). This property is used in practical applications such as data storage [19].

An expression for the first-order uniaxial anisotropy potential energy density with the axis \mathbf{k}_a and unit magnetization \mathbf{M} is given by:

$$E_a = -K(\mathbf{M} \cdot \mathbf{k}_a)^2 \quad (2.18)$$

with K being anisotropy coefficient.

The corresponding effective field then can be derived as:

$$\mathbf{H}_a = \frac{2K}{M_s} (\mathbf{M} \cdot \mathbf{k}_a) \mathbf{k}_a. \quad (2.19)$$

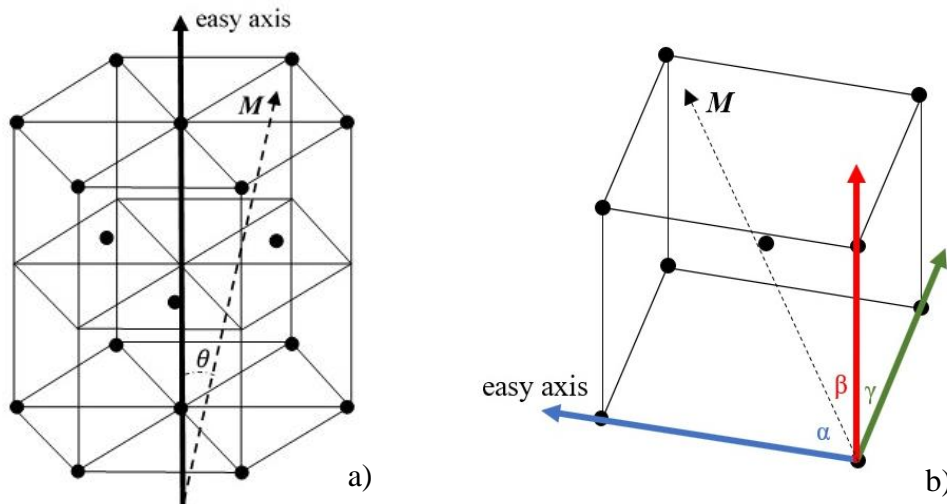


Figure 2.5: a) Uniaxial anisotropy: hexagonal close packed crystal structure with a single magnetocrystalline anisotropy easy axis. b) Cubic anisotropy: body centered cubic crystal structure with three anisotropy easy axes.

Uniaxial anisotropy usually occurs in the crystal systems which have an axis of high symmetry, such as threefold, fourfold and sixfold symmetry [20, 21].

Another anisotropy type is cubic anisotropy, which is defined in cubic crystals that have three crystal axes (figure 2.5 b) [22]. The corresponding energy density is:

$$E_a = K_1(\alpha^2\beta^2 + \beta^2\gamma^2 + \gamma^2\alpha^2) + K_2(\alpha^2\beta^2\gamma^2), \quad (2.20)$$

where α , β , γ are respectively cosines of the angles between the magnetization and the three crystal axes, which are called direction cosines, the three axes are perpendicular to each other.

2.3.4 Exchange interaction

Pierre Weiss proposed the first modern theory of ferromagnetism in 1906 [23]. The idea was that there is a ‘molecular field’ proportional to the ferromagnetic magnetization in the sample, leading to spontaneous alignment of the neighboring magnetic moments. In fact, such field does not really exist, the origin of ferromagnetism is the exchange interaction, it is a short-ranged interaction which reflects the electronic Coulomb repulsion and Pauli exclusion principle [24]. Two electrons are forbidden from occupying the same quantum state and there is an energy difference between the $\uparrow\uparrow$ and $\uparrow\downarrow$ configuration of spins of neighboring atoms. We can write the exchange interaction energy using the Heisenberg Hamiltonian [25]:

$$E_{ex} = -J_{ex}\mathbf{S}_1 \cdot \mathbf{S}_2, \quad (2.21)$$

where \mathbf{S}_1 and \mathbf{S}_2 are dimensionless spin operators and J_{ex} is exchange constant that characterizes the strength of exchange interactions. The exchange type and the magnetic property of the material are determined by J_{ex} . The sign of $J_{ex} > 0$ indicates a ferromagnetic interaction, i.e. a parallel alignment of two spins minimizes the exchange energy and $J_{ex} < 0$

indicates an antiferromagnetic interaction, i.e. antiparallel spin alignment. The exchange interaction also leads to the generation of magnetic domains.



Figure 2.6: a) Ferromagnetic interaction, $J_{ex} > 0$ favors parallel alignment of neighboring spins. b) Antiferromagnetic interaction, $J_{ex} < 0$ favors antiparallel alignment of neighboring spins.

In micromagnetic simulations, we assume continuous energies and compute magnetization at the mesh nodes of the finite element model rather than simulate the behaviors of atomic and electronic scale. The continuous form of the exchange interaction energy is derived from (2.21):

$$E_{ex} = \int_V A(\nabla \mathbf{M})^2 d^3 \mathbf{r}, \quad (2.22)$$

where A is the exchange stiffness constant dependent to J_{ex} . Then we take the derivative of the energy relative to magnetization to get the exchange field:

$$\mathbf{H}_{ex} = \frac{2A}{M_s} \nabla^2 \mathbf{M}, \quad (2.23)$$

where M_s is saturation magnetization.

2.4 Domain walls

A region in which the magnetization orientation is uniform is called magnetic domain, and domain walls are the interfaces that separate different domains. Domain walls are a result of the competition between exchange energy, anisotropy, and magnetostatic interactions.

Imagine that the magnetic moments change their direction abruptly, occurring from one atom to the next one, and both are parallel and antiparallel to the anisotropy easy axis (figure 2.7 a). As discussed in section 2.3.4, the exchange energy in ferromagnets is maximized when adjacent spins are antiparallel, therefore, the wall has a large exchange energy and it can be decreased if the 180° change in magnetic moment direction occurs gradually over several atoms. However, in such a case, more magnetic moments point away from the easy axis and the magnetocrystalline anisotropy energy within the wall is higher. In addition, magnetostatic interactions tend to misalign the spins. Domain wall is the result of this competition, and it ends up an interfacial region with definite width and structure when the total energy reaches the minimum (figure 2.7 b).

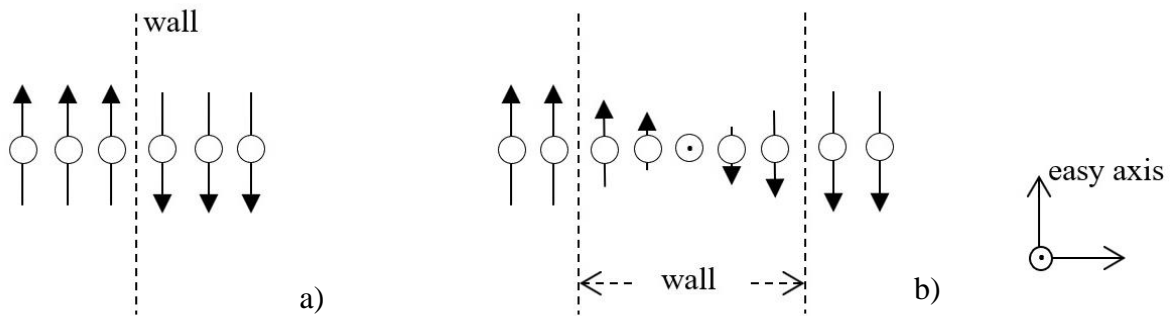


Figure 2.7: Domain wall in a system with uniaxial anisotropy. a) Hypothetical 180° domain wall with abrupt magnetization change. b) Structure of a 180° domain wall, gradual change of magnetization orientation where anisotropy energy and exchange energy balance each other.

Domain walls have two major categories, called Bloch and Néel domain walls. Bloch wall was named for Felix Bloch, who conducted the first theoretical examination of domain walls [26]. In Bloch walls, the axis about which the magnetization varies from one direction of easy axis to the other is in the plane of magnetization on both sides, meaning that the

magnetization within the wall points out of the plane (figure 2.8 a). When the thickness of the sample and the domain wall in it are comparable, the potential energy generated by the free dipoles on the surface of the domain wall becomes significant. This energy makes the magnetizations rotate in the plane of the thin sample, which means that the magnetization vectors in and out of the domain wall are in the same plane (figure 2.8 b). Such a wall structure is called Néel wall, after French physicist Louis Néel [27].

Like other kinds of interfaces, domain wall has energy per unit area of its surface. It is expressed by the sum of the exchange energy density and anisotropy energy density, then integrated over the wall thickness:

$$\sigma_{dw} = \int_{-\infty}^{\infty} \left[A \left(\frac{d\theta}{dx} \right)^2 + E_a(\theta) \right] dx \quad (2.24)$$

where θ is the angle between magnetization orientation and the easy axes, E_a is the anisotropy energy density.

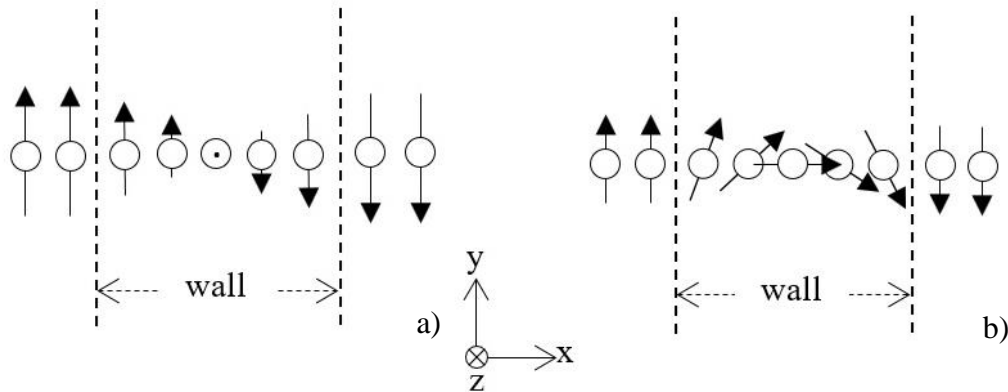


Figure 2.8: Two kinds of magnetic tracks in domain wall with a single anisotropy easy axis in y direction. a) Example of a 180° Bloch domain wall, the magnetization rotates between two opposite directions of the easy axis about the x axis. b) Example of a 180° Néel domain wall, the magnetization rotates between two opposite directions of the easy axis about the z axis.

Domain wall naturally minimizes its total energy, until that the exchange and anisotropy energies balance each other everywhere within the wall, $A \left(\frac{d\theta}{dx} \right)^2 = E_a(\theta)$ where uniaxial anisotropy $E_a(\theta) = K_a \sin^2 \theta$, then we can get the relation between x and θ (figure 2.9):

$$x = \sqrt{\frac{A}{K_a}} \ln \left(\tan \frac{\theta}{2} \right), \quad (2.25)$$

the effective wall thickness:

$$\delta_{dw} = \pi \sqrt{\frac{A}{K_a}}, \quad (2.26)$$

and the energy per unit area of wall surface at equilibrium:

$$\sigma_{dw} = 4\sqrt{AK_a}. \quad (2.27)$$

Typically, the wall thickness spans from a sub-nanometer to hundreds of nanometers [28].

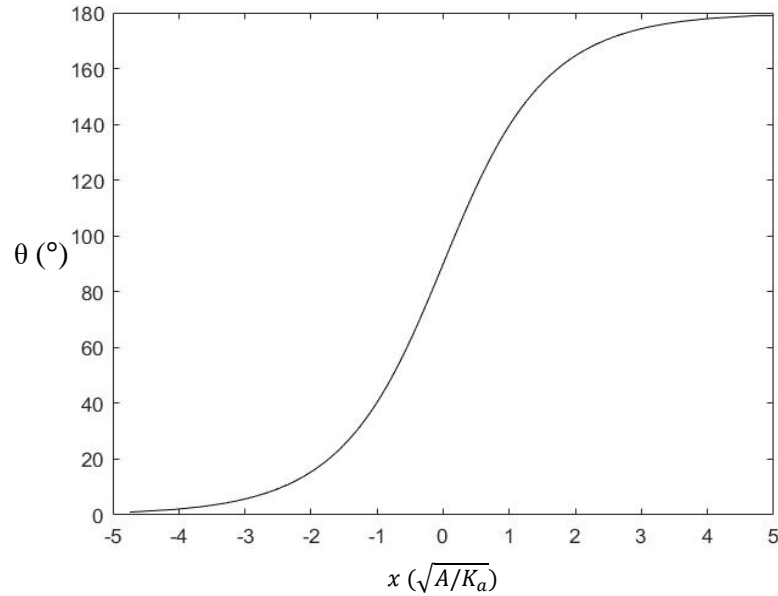


Figure 2.9: Variation of the angle between magnetization and the easy axis with respect to the position in the domain wall, x , in unit of $\sqrt{A/K_a}$, the position $x = 0$ is the center of the wall.

Chapter 3

Spin dynamics in nanomagnetic structures

The new generation of non-volatile random-access memory, magnetoresistive random-access memory(MRAM), began its development in the 1960s [29] and research on it surged after the introduction of giant magnetoresistance in 1988 [2][3]. Different from other conventional RAMs, data in MRAMs is stored in magnetic elements instead of electric charge or current. In the basic configuration, the magnetic elements include two ferromagnetic layers separated by a thin non-magnetic layer, one of which is a permanent magnet whose magnetization is fixed in a particular orientation, while the other layer's magnetization can be changed by an applied magnetic field.

Applying magnetic field is the way to write MRAM and reading is accomplished through measurement of the electrical resistance of the storage element. Due to the tunnel magnetoresistance effect, the electrical resistance changes depending on the relative states of the references and free layers. Because of MRAM's fast switching, reliability, scalability, and nonvolatility, its proponents believe that it may dominate the future memory market.

Spin transfer torque MRAM(STT-MRAM) is a new advanced memory type that uses spin-polarized current to write MRAM instead of magnetic field, as was proposed by Slonczewski [30] and Berger [31] in 1996. The STT effect is the key of this technology. When

current flows through a magnetically inhomogeneous structure, the current is spin polarized and this polarization exerts a spin torque on the local magnetic moments, leading to the magnetization reversal.

In micromagnetics, the Slonczewski's model [32] is frequently used for the simulation of STT effects in multi-layer structure and Zhang & Li model [33] is used for structures with domain walls. However, both models do not describe the spin dynamics in magnetic structures. In this chapter, spin diffusion model, a physical model that enables explicit calculation of spin accumulation dynamics, is introduced. Brief introduction of spin-polarization, spin valve and STT is also presented before that. Finally, the numerical implementation of spin diffusion model is examined through numerical experiments.

3.1 Spin polarization

An electron carries not only its charge, but also an angular momentum $\hbar m_s$, where $m_s = \pm 1/2$ for the spin down and up states, \downarrow and \uparrow , respectively. The corresponding magnetic moment is proportional to the angular momentum, $\mu_s = \gamma \hbar m_s$, where γ is gyromagnetic ratio. Electronic spin can be flipped between \downarrow and \uparrow states by scattering processes. The spin flipping scattering is relatively rarer than normal momentum changing scattering [34] so that the conduction of electrons can be thought of going through two parallel channels for \downarrow and \uparrow separately, this two-current model was proposed by Mott in 1936 [35].

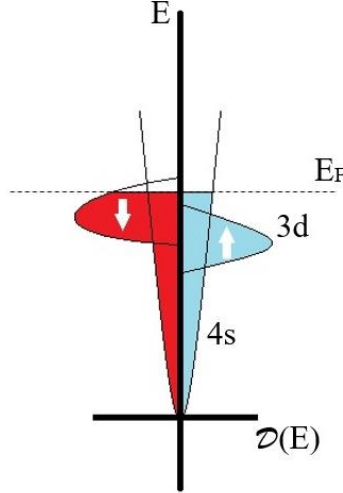


Figure 3.1: Schematic representation of the density of states function in 3d and 4s energy band of nickel where blue part is for \uparrow state and red part is for \downarrow state. Exchange energy splitting occurs in 3d band, \uparrow states are fully occupied while \downarrow states with higher energy are incompletely occupied.

In normal metals, both the electronic band structure and the occupancy of spin up and spin down states are equal. However, due to a strong exchange interaction, the electronic band structure of ferromagnets splits. As an example, for nickel, which is a ferromagnetic metal, exchange splitting exists in the 3d band [36], $3d\uparrow$ band is fully occupied, but the \downarrow electrons can be excited into empty $3d\downarrow$ states at the Fermi level (figure 3.1). This population imbalance of spin up and spin down electrons results in a non-zero spin polarization. Also, since the frequency of spin flipping scattering is proportional to the density of unoccupied states at the Fermi surface [37], \downarrow electrons are more likely to be scattered and their transport is more impeded, further reinforcing the spin population imbalance. The polarization, P , of an ensemble of electrons can be described in terms of the population density of the electrons in spin up state n_{\uparrow} and spin down state n_{\downarrow} :

$$P = \frac{n \uparrow - n \downarrow}{n \uparrow + n \downarrow}. \quad (3.1)$$

When all electrons are in the same spin state, $P=1$, they are completely spin polarized. When \uparrow and \downarrow states are equally likely to be occupied, $P=0$, the electrons are unpolarized. The definition of spin polarization can also be used in electric current, a spin-polarized current is a flow of electrons whose spin population is in imbalance.

3.2 Spin valve and spin transfer torque

Consider a normal metal / ferromagnet / normal metal junction (NM1/FM/NM2) through which electrons flow from left to right (figure 3.2). When the electrons exit the left-hand-side normal metals(NM1) and enter the ferromagnets, the initially unpolarized current is spin polarized due to the density imbalance of spin states and the spin dependent difference of scattering frequency in ferromagnets. As they exit the ferromagnet and enter the right-hand-side NM2, the spin polarization builds up at the interface. This is referred to as spin accumulation [34, 38, 39] and it is usually measured as spin splitting voltage in experiments. The polarization then declines with increasing distance from ferromagnet because majority spin carriers scatter more in normal metals until the population of two spin states goes back to balance [40].

Spin polarized current also exists in NM1. The difference in scattering frequency of spin up and spin down electrons between normal metals and ferromagnets makes minority spin carriers more likely to be reflected at the interface [40], which results in a spin accumulation that declines with increasing distance from ferromagnet.

The total angular momentum of the electrons and lattice system must be conserved, which means that a gain of angular momentum of electric current must be balanced by the loss of angular momentum of lattice. Therefore, the underlying physics of the polarization of electric current is, in fact, the transfer of angular momentum from ferromagnet lattice to electron flow. It implies that angular momentum can also be transferred from spin polarized current to lattice, switching the magnetization of the ferromagnet. This effect is known as spin transfer torque (STT) effect [30, 31].

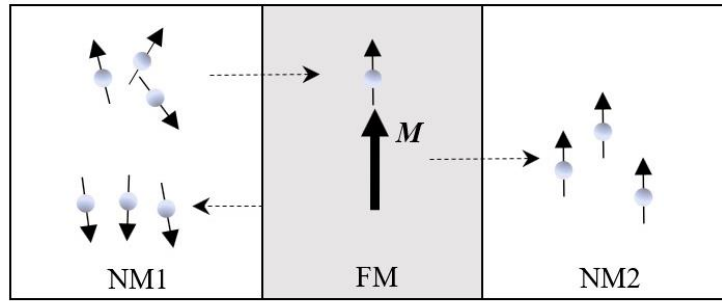


Figure 3.2: A normal metal / ferromagnet / normal metal junction in which the electrons flow from the left to the right. The electrons are spin polarized in both metallic layers.

Now we add two more layers to the junction to make it a normal metal / ferromagnet / normal metal / ferromagnet / normal metal spin valve (figure 3.3). Generally, one of the ferromagnets is set to be thicker (FM1) and the other one is thinner (FM2). The magnetization in thicker ferromagnet FM1 is large enough to resist the influence from the STT effect, so FM1 is only used to polarize the electric current. When a voltage is applied to this spin valve, the current polarized in appropriate orientation by FM1 switches the magnetic state of FM2 and the rate of the supplementation of angular momentum from spin current must be able to compensate the dissipation in Larmor precession of moments.

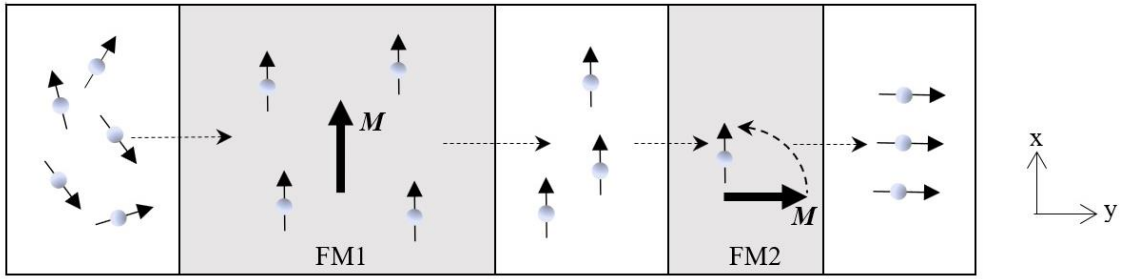


Figure 3.3: A normal metal / ferromagnet / normal metal / ferromagnet / normal metal spin valve where FM1 layer is magnetized in x direction and FM2 layer is magnetized in y direction. The electrons polarized by FM1 transfer angular momentum to the lattice of FM2, changing its magnetization orientation.

For example, we can assume that FM1 is initially magnetized in the x direction and FM2 in the y direction. Suppose the electrons are moving in the z direction from FM1 to FM2, at the interface between FM1 and the normal metal, the randomly polarized incident electrons are either reflected or transmitted, but those with majority spins of FM1 are more easily transmitted. The electrons that enter FM1 are subject to a strong exchange field in the x direction, forcing them to precess at Larmor frequency. At the time they leave FM1, their y and z component of the spin magnetic moment are dephased [41, 42, 43], or in other words, the corresponding momentum is transferred to the lattice. The transfer rate can be expressed as $j\hbar P \sin \theta / (2e)$, where j is current density and θ is the angle between the moment and the magnetization. Another mechanism is based on the great difference between the mean free path of majority and minority spin electrons. The minority spin electrons' angular momentum is transferred by scattering within the first nanometers while the majority ones can transport much longer before scattering [44].

When the electrons with angular momentum in the x direction arrive at FM2, their momentum is absorbed by the lattice and they precess about the y axis as was just described. Differently, the torque exerted on FM2 tends to rotate the magnetization toward the orientation of the incoming current polarization, leading to the parallel configuration of FM1 and FM2.

3.3 Spin transfer torque in micromagnetics

When the STT effect is taken into consideration, an additional term must be added to the LLG equation:

$$\frac{d\mathbf{M}}{dt} = -\frac{\gamma}{1+\alpha^2}(\mathbf{M} \times \mathbf{H}_{eff}) - \frac{\alpha\gamma}{1+\alpha^2}\mathbf{M} \times \mathbf{M} \times \mathbf{H}_{eff} + \mathbf{L}, \quad (3.2)$$

in which \mathbf{L} represents the effective spin transfer torque acted on the magnetization \mathbf{M} .

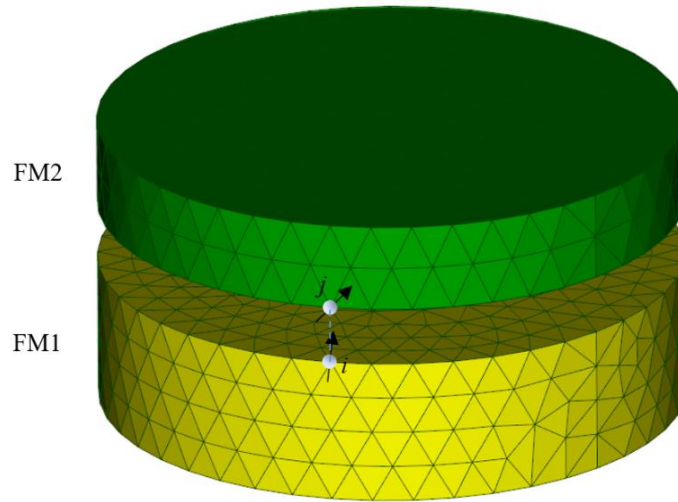


Figure 3.4: Tetrahedral finite element mesh of two magnetic layers separated by a metallic spacer (not shown) for calculation of STT in Slonczewski model, a pair of nodes i and j is shown.

There are two frequently used models for the STT effect in micromagnetics: one is Slonczewski's model and the other is Zhang & Li's model. In Slonczewski's model [32] (figure

3.4), the magnetization in the layer for polarization (FM1) is assumed to be fixed, spin transfer torque is computed at each node i on the interface of free layer (FM2) by the equation:

$$\mathbf{L}_i^{STT} = \eta(\theta_{ij}) \frac{\hbar J_e}{2e t_i} \mathbf{M}_i \times \mathbf{M}_i \times \mathbf{M}_j, \quad (3.3)$$

where node j is directly opposed to the node i across the spacer layer, J_e is electric current density, t_i is the effective depth over which spin transfer torque is distributed at node i , \mathbf{M}_i and \mathbf{M}_j are unit magnetization at node i and j respectively, $\eta(\theta_{ij})$ is angular coefficient related to the angle θ_{ij} between magnetization orientation at node i and j :

$$\eta(\theta_{ij}) = \frac{q^+}{A + B \cos \theta_{ij}} + \frac{q^-}{A - B \cos \theta_{ij}}, \quad (3.4)$$

coefficients A , B , q^+ , q^- all depend on the geometry of the system.

Slonczewski model is a straightforward way to deal with spin transfer torque in multi-layered structures, but its fixed magnetization in pinned layer makes it not fit for varying magnetization configuration such as domain wall motion, while Zhang & Li model [33] is good for describing spin transfer torque in the domain wall case. The model is a simplified version of the spin diffusion model discussed in section 3.4 with the assumptions that the spin accumulation varies slowly in space and that the spin transfer torque is computed under spin equilibrium. The torque exerted by current of density \mathbf{J}_e is expressed as:

$$L^{STT} = \frac{1}{1 + \xi^2} \frac{\lambda_j^2 \beta \mu_B}{2D_0 e} (-\mathbf{M} \times [\mathbf{M} \times (\mathbf{J}_e \cdot \nabla) \mathbf{M}] - \xi \mathbf{M} \times (\mathbf{J}_e \cdot \nabla) \mathbf{M}), \quad (3.5)$$

where $\lambda_j = \sqrt{2\hbar D_0 / J_{ex}}$ with J_{ex} being exchange constant between conducting electrons and magnetization, D_0 is electron diffusion constant, β is spin polarization parameter for the

conductivity, and $\xi = \lambda_j^2 / \lambda_{sf}^2$ with λ_{sf} being related to spin flipping relaxation time τ_{sf} via

$$\lambda_{sf} = \sqrt{2D_0\tau_{sf}}.$$

Zhang & Li model loses its accuracy when dealing with magnetic multi-layer structure since the assumption that the spin accumulation varies little in space is violated at the interfaces between non-magnetic and magnetic layers where the spin polarization is built up abruptly.

Whichever model is used to solve for the magnetization dynamics equation, we only need to directly compute the spin transfer torque without knowing spin polarization. Another explicit way is to get spin accumulation of each iterative step first and then calculate the spin transfer torque. A spin diffusion model is required to accomplish this task.

3.4 Spin diffusion model

3.4.1 Continuous formulation

A spin diffusion model was first presented in 2002 [45]. In this model, spin accumulation is a vector variable that represents the spin polarization acting torque on background magnetization in semiclassical physical models. Spin accumulation is measured in the unit of a magnetic field and the spin transfer torque can be calculated as $\mathbf{s} \times \mathbf{M}$, similar to an applied magnetic field.

The equation that describes the motion of spin accumulation \mathbf{s} in three dimensions is:

$$\frac{\partial \mathbf{s}}{\partial t} = -\nabla \cdot \mathbf{J}_s - 2D_0 \left[\frac{\mathbf{s}}{\lambda_{sf}^2} + \frac{\mathbf{s} \times \mathbf{M}}{\lambda_j^2} \right], \quad (3.6)$$

for a given electric current density \mathbf{J}_e , the matrix-valued spin current \mathbf{J}_s is expressed as:

$$\mathbf{J}_s = \frac{\beta\mu_B}{e} \mathbf{M} \otimes \mathbf{J}_e - 2D_0[\nabla \mathbf{s} - \beta\beta' \mathbf{M} \otimes ((\nabla \mathbf{s})^T \mathbf{M})], \quad (3.7)$$

where $\lambda_j = \sqrt{2\hbar D_0 / J_{ex}}$ and $\lambda_{sf} = \sqrt{2D_0 \tau_{sf}}$, which are same as those in (3.5), D_0 is diffusion constant, β and β' are defined as spin polarization parameters for electric conduction and electron diffusion, respectively. Here, $\mathbf{a} \otimes \mathbf{b} = \mathbf{ab}^T$ is the outer product of two vectors, $\nabla \mathbf{s}$ is Jacobian matrix of \mathbf{s} , that is:

$$\nabla \mathbf{s} = \begin{pmatrix} \frac{\partial s_x}{\partial x} & \frac{\partial s_x}{\partial y} & \frac{\partial s_x}{\partial z} \\ \frac{\partial s_y}{\partial x} & \frac{\partial s_y}{\partial y} & \frac{\partial s_y}{\partial z} \\ \frac{\partial s_z}{\partial x} & \frac{\partial s_z}{\partial y} & \frac{\partial s_z}{\partial z} \end{pmatrix}, \quad (3.8)$$

and divergence of a 3×3 matrix $\bar{\bar{A}}$ is defined as:

$$\nabla \cdot \bar{\bar{A}} = \begin{pmatrix} \frac{\partial A_{11}}{\partial x} + \frac{\partial A_{21}}{\partial y} + \frac{\partial A_{31}}{\partial z} \\ \frac{\partial A_{12}}{\partial x} + \frac{\partial A_{22}}{\partial y} + \frac{\partial A_{32}}{\partial z} \\ \frac{\partial A_{13}}{\partial x} + \frac{\partial A_{23}}{\partial y} + \frac{\partial A_{33}}{\partial z} \end{pmatrix}. \quad (3.9)$$

We can find that the left-hand side of (3.6) is the time dependence of the spin accumulation and the right-hand side has the Laplacian of spin accumulation $\nabla^2 \mathbf{s}$ after replacing \mathbf{J}_s in (3.6) with (3.7), so (3.6) is a diffusion equation of spin accumulation. The term $\mathbf{M} \otimes \mathbf{J}_e$ represents the source of spin accumulation, describing the build-up process in varying magnetization. The terms $2D_0 \mathbf{s} / \lambda_{sf}^2$ and $2D_0 (\mathbf{s} \times \mathbf{M}) / \lambda_j^2$ are contributed by the polarization dissipation resulted from spin flipping scattering and by the STT effect between background magnetization respectively.

3.4.2 Discrete node-based formulation

One approach to discretize the continuous spin diffusion equations is to obtain all terms at the nodes of the mesh and have equations defined at the nodes. First, we can make use of tensor identities about vectors \mathbf{u} , \mathbf{v} and matrix $\bar{\bar{A}}$:

$$\nabla \cdot (\mathbf{u} \otimes \mathbf{v}) = (\nabla \mathbf{u})\mathbf{v} + (\nabla \cdot \mathbf{v})\mathbf{u} \quad (3.10)$$

and

$$\nabla \cdot (\bar{\bar{A}}\mathbf{u}) = \mathbf{u} \cdot (\nabla \cdot \bar{\bar{A}}^T) + tr[\bar{\bar{A}}(\nabla \mathbf{u})] \quad (3.11)$$

to rewrite (3.6) and (3.7) into:

$$\begin{aligned} \frac{\partial \mathbf{s}}{\partial t} = & -\frac{\beta\mu_B}{e} [(\nabla \mathbf{M})\mathbf{J}_e + (\nabla \cdot \mathbf{J}_e)\mathbf{M}] + 2D_0 \nabla^2 \mathbf{s} - 2D_0 \beta \beta' (\nabla \mathbf{M}) [(\nabla \mathbf{s})^T \mathbf{M}] \\ & - 2D_0 \beta \beta' \{ \mathbf{M} \cdot (\nabla^2 \mathbf{s}) + tr[(\nabla \mathbf{s})^T (\nabla \mathbf{M})] \} \mathbf{M} - 2D_0 \frac{\mathbf{s}}{\lambda_{sf}^2} - 2D_0 \frac{\mathbf{s} \times \mathbf{M}}{\lambda_j^2}. \end{aligned} \quad (3.12)$$

In our formulation, the spin accumulation is represented via finite element model with linear basis functions ξ . It can be shown that the Laplacian of a vector variable can be derived into element discretized form via the box method [46, page 57-59]:

$$\nabla^2 \mathbf{s} \big|_p = -\frac{1}{V_p} \sum_{l=1}^M \sum_{k=1}^4 (\nabla \xi_p^l \cdot \nabla \xi_k^l) V_l \mathbf{s}_k, \quad (3.13)$$

the calculation of $\nabla^2 \mathbf{s}$ at node p iterates over all M elements surrounding this node, and in each element l , all its vertices are gone through from $k = 1$ to 4. Here, V_p is the effective volume of node p defined as:

$$V_p = \frac{1}{4} \sum_{l=1}^M V_l, \quad (3.14)$$

with V_l being the volume of element l . Based on the geometry, the general expression of the gradient of linear basis function is formulated as:

$$\nabla \xi_q^l = \frac{\mathbf{v}_q^l}{|\mathbf{v}_q^l|^2}. \quad (3.15)$$

The vector \mathbf{v}_q^l points to node q from a point on the opposing tetrahedral face to which the vector is perpendicular, it is written as:

$$\mathbf{v}_q^l = [(\mathbf{r}_q^l - \mathbf{r}_r^l) \cdot \mathbf{n}_{rst}^l] \mathbf{n}_{rst}^l \quad (3.16)$$

with position vectors $\mathbf{r}_q^l, \mathbf{r}_r^l, \mathbf{r}_s^l, \mathbf{r}_t^l$ of the four vertices of tetrahedron l , and

$$\mathbf{n}_{rst}^l = \frac{(\mathbf{r}_r^l - \mathbf{r}_s^l) \times (\mathbf{r}_r^l - \mathbf{r}_t^l)}{|(\mathbf{r}_r^l - \mathbf{r}_s^l) \times (\mathbf{r}_r^l - \mathbf{r}_t^l)|}. \quad (3.17)$$

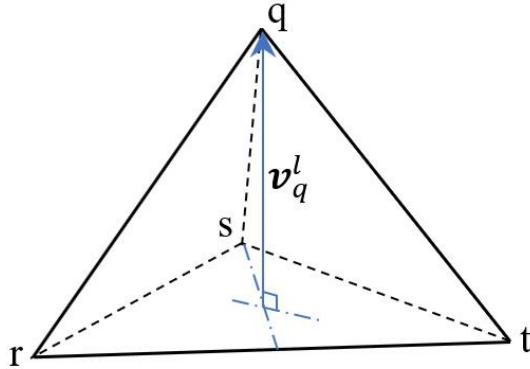


Figure 3.5: Tetrahedron l with four vertices q, r, s, t , appearing in (3.15) to (3.17). The vector \mathbf{v}_q^l is perpendicular to the plane rst .

In our work, we use implicit Euler scheme to solve for the spin accumulation \mathbf{s}^{k+1} at the next time-step. Assuming the right-hand side of the equation (3.12) to be $\mathbf{f}(\mathbf{M}, \mathbf{s}^{k+1})$, we get its temporally discretized form:

$$\frac{\mathbf{s}^{k+1} - \mathbf{s}^k}{\tau} = \mathbf{f}(\mathbf{M}, \mathbf{s}^{k+1}) \quad (3.18)$$

with τ being timestep, or

$$\mathbf{s}^{k+1} - \tau \mathbf{f}(\mathbf{M}, \mathbf{s}^{k+1}) = \mathbf{s}^k \quad (3.19)$$

after reorganization.

It is easy to find that the left-hand side of (3.19) is the linear combination of s_x, s_y, s_z at the time-step $k+1$ and that the right-hand side is a known vector, so we are solving a large system of linear equations, which can be expressed as:

$$\bar{\bar{A}}_{3N \times 3N} \begin{pmatrix} s_{1x} \\ s_{2x} \\ \vdots \\ s_{Nx} \\ s_{1y} \\ \vdots \\ s_{Ny} \\ s_{1z} \\ \vdots \\ s_{Nz} \end{pmatrix}^{k+1} = \mathbf{b}_{3N \times 1}^k, \quad (3.20)$$

where $\bar{\bar{A}}_{3N \times 3N}$ is a sparse matrix.

Besides the description of the diffusion of spin accumulation, a continuity condition that spin current \mathbf{J}_s is continuous across the interface [47], must be added at the interfaces between two different materials as well, the condition is expressed by the equation:

$$\mathbf{J}_{s,i}^{in} \cdot \mathbf{n}_i = \mathbf{J}_{s,i}^{out} \cdot \mathbf{n}_i, \quad (3.21)$$

or in more detail:

$$\begin{aligned} 2D_0^{in} [(\nabla \mathbf{s}^{in})_i \cdot \mathbf{n}_i] - 2D_0^{out} [(\nabla \mathbf{s}^{out})_i \cdot \mathbf{n}_i] - 2D_0^{in} \beta \beta' \{ \mathbf{M}_i^{in} \cdot [(\nabla \mathbf{s}^{in})_i \cdot \mathbf{n}_i] \} \mathbf{M}_i^{in} \\ = \frac{\beta \mu_B}{e} (\mathbf{J}_{e,i} \cdot \mathbf{n}_i) \mathbf{M}_i^{in}, \end{aligned} \quad (3.22)$$

where superscripts *in* and *out* means the \mathbf{s} , \mathbf{M} or D_0 inside and outside the magnetic material respectively, subscript i indicates the variable at the node i and it goes over all nodes on all interfaces between ferromagnetic and nonmagnetic layers. \mathbf{n}_i is the unit normal vector that perpendicular to the interface at node i .

The spin current continuity equation implies the generation of the polarization at the interfaces, the difference between the spin accumulation on the both sides of the interface compensates the value of term $\frac{\beta\mu_B}{e} (\mathbf{J}_{e,i} \cdot \mathbf{n}_i) \mathbf{M}_i^{in}$.

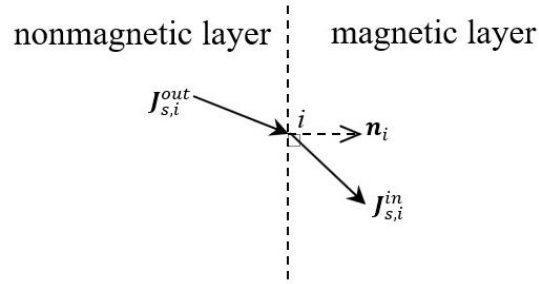


Figure 3.6: Schematic representation of (3.21). Spin current \mathbf{J}_s flows from the nonmagnetic layer to the magnetic layer, \mathbf{n}_i is the unit vector perpendicular to the interface at the node i .

In order to simulate the spin dynamics, we must solve (3.19) and (3.22) simultaneously. Assuming there are N nodes in the system, we will need $3N$ equations to solve $3N$ unknown variables for the three components in the x , y , z directions of the spin accumulation at each node. These equations are composed of the equation (3.22) applied on all nodes on the interfaces and of the equation (3.19) applied on the others inside the volumes.

3.4.3 Discrete element-based formulation — weak formulation

Another discretization approach is based on each element. It solves the weak form of the spin diffusion equation using Galerkin method. We multiply both sides of the equation (3.6) by a test vector function $\boldsymbol{\varphi}$ and integrate it over the entire system. The new equation is called weak formulation and its solution is called weak solution. Weak solutions are not necessarily differentiable, so the weak formulation of the differential equations can be solved more easily and conveniently, especially for those that do not admit completely smooth solutions.

Then invoking the identities

$$\alpha \nabla \phi \cdot \nabla \psi = \nabla \cdot (\alpha \psi \nabla \phi) - \psi \nabla \cdot (\alpha \nabla \phi) \quad (3.23)$$

$$\nabla \cdot (\psi \boldsymbol{\varphi}) = \psi (\nabla \cdot \boldsymbol{\varphi}) + \boldsymbol{\varphi} \cdot (\nabla \psi) \quad (3.24)$$

and Gauss's theorem

$$\iiint_V \nabla \cdot \boldsymbol{\varphi} \, dr^3 = \iint_S \boldsymbol{\varphi} \cdot \mathbf{n} \, dr^2, \quad (3.25)$$

we can convert equation (3.6) into the weak formulation without second order differential [48]:

$$\begin{aligned} & \iiint_V \frac{\partial \mathbf{s}}{\partial t} \cdot \boldsymbol{\varphi} \, dr^3 + \frac{2D_0}{\lambda_{sf}^2} \iiint_V \mathbf{s} \cdot \boldsymbol{\varphi} \, dr^3 + 2D_0 \iiint_V \nabla \mathbf{s} : \nabla \boldsymbol{\varphi} \, dr^3 \\ & - 2D_0 \beta \beta' \iiint_{V_{mag}} \{\mathbf{m} \otimes [(\nabla \mathbf{s})^T \cdot \mathbf{m}]\} : \nabla \boldsymbol{\varphi} \, dr^3 + \frac{2D_0}{\lambda_j^2} \iiint_{V_{mag}} (\mathbf{s} \times \mathbf{m}) \cdot \boldsymbol{\varphi} \, dr^3 \\ & = \frac{\beta \mu_B}{e} \iiint_{V_{mag}} (\mathbf{m} \otimes \mathbf{J}_e) : \nabla \boldsymbol{\varphi} \, dr^3 - \frac{\beta \mu_B}{e} \iint_{S_{mag}^{outer}} (\mathbf{J}_e \cdot \mathbf{n}) \cdot (\mathbf{m} \cdot \boldsymbol{\varphi}) \, dr^2, \end{aligned} \quad (3.26)$$

where V_{mag} indicates the integral over only magnetic volumes and S_{mag}^{outer} indicates the integral over all outer surfaces of the magnetic volumes, $\mathbf{A} : \mathbf{B} = \sum_{i,j=1}^3 \mathbf{A}_{ij} \cdot \mathbf{B}_{ij}$ is the Frobenius inner product of two matrix.

Similarly, we also use implicit Euler scheme here, and choose the spin accumulation to be solved \mathbf{s}^{k+1} as the test function then interpolate it over each finite element. The spin accumulation inside the element e is expressed as:

$$\mathbf{s}_e^{k+1} = \sum_{i=1}^4 N_i^e \cdot \mathbf{s}_{e,i}^{k+1}, \quad (3.27)$$

where N_i^e is the linear interpolation formula at the i -th node of the element e . Now we use equations (3.18) and (3.27) to rewrite the equation (3.26) in discretized form:

$$\begin{aligned} & \sum_{i=1}^4 \sum_{j=1}^4 \mathbf{s}_{e,i}^{k+1} \cdot \mathbf{s}_{e,j}^{k+1} \iiint_V \left(\frac{1}{\tau} + \frac{2D_0}{\lambda_{sf}^2} \right) N_i^e \cdot N_j^e + 2D_0 \nabla N_i^e \cdot \nabla N_j^e d\mathbf{r}^3 \\ & - 2D_0 \beta \beta' \sum_{i=1}^4 \sum_{j=1}^4 \{ (\mathbf{s}^{k+1})_j \cdot \mathbf{m} \otimes \mathbf{m} \}^e \mathbf{s}_{e,i}^{k+1} \iiint_{V_{mag}} \nabla N_i^e \cdot \nabla N_j^e d\mathbf{r}^3 \\ & + \frac{2D_0}{\lambda_j^2} \sum_{i=1}^4 \sum_{j=1}^4 \mathbf{s}_{e,i}^{k+1} \cdot (\mathbf{s}^{k+1} \times \mathbf{m})_j \iiint_{V_{mag}} N_i^e \cdot N_j^e d\mathbf{r}^3 \\ & = \frac{\beta \mu_B}{e} \sum_{i=1}^4 [(\mathbf{J}_e \otimes \mathbf{m}) \cdot \mathbf{s}_{e,i}^{k+1}] \cdot \iiint_{V_{mag}} \nabla N_i^e d\mathbf{r}^3 \\ & - \frac{\beta \mu_B}{e} \sum_{i=1}^4 (\mathbf{J}_e \cdot \mathbf{n}) \cdot (\mathbf{m} \cdot \mathbf{s}^{k+1})_i^e \iint_{S_{mag}^{outer}} N_i^e d\mathbf{r}^2 \\ & + \frac{1}{\tau} \sum_{i=1}^4 (\mathbf{s}^k \cdot \mathbf{s}^{k+1})_i^e \iiint_{V_{mag}} N_i^e d\mathbf{r}^3 \end{aligned} \quad (3.28)$$

where the integrals of the interpolation formulas and their gradient terms can be calculated using Ritz method [49, page 167-173].

Mathematically, equation (3.28) can be simply expressed as:

$$(\mathbf{s}^{k+1})_e^T \cdot \bar{\mathbf{K}}_{12 \times 12}^e \mathbf{s}_e^{k+1} = (\mathbf{s}^{k+1})_e^T \cdot \mathbf{b}_{12 \times 1}^e, \quad (3.29)$$

then iterate equation (3.29) over all M elements to assemble matrix $\bar{\bar{\mathbf{K}}}_{3N \times 3N} = \sum_{e=1}^M \bar{\bar{\mathbf{K}}}_{12 \times 12}^e$ and vector $\mathbf{b}_{3N \times 1} = \sum_{e=1}^M \mathbf{b}_{12 \times 1}^e$ for all N nodes, eventually, solve the system of linear equations:

$$\bar{\bar{\mathbf{K}}}_{3N \times 3N} \mathbf{s}^{k+1} = \mathbf{b}_{3N \times 1}. \quad (3.30)$$

In this work, we use an iterative method, generalized minimal residual method (GMRES), to solve the system of linear equations. Since the eigenvalues of the matrix differ a lot, the incomplete LU factorization, including ILU(0) and ILUT, and the inverse of the matrix are calculated before computation, respectively as preconditioners to speed up the convergence. The computational performance of the preconditioners is presented in the next section. Also, it is shown that node-based and element-based computational methods are both able to solve spin diffusion equation, the difference between their solutions is numerically acceptable.

3.4.4 Spin diffusion model coupled with the LLG equation

The magnetization dynamics with the spin transfer torque effect is governed by the LLG equation coupled with spin accumulation \mathbf{s} :

$$\frac{d\mathbf{M}}{dt} = -\gamma \mathbf{M} \times (\mathbf{H}_{eff} + \frac{J}{\hbar \gamma M_s} \mathbf{s}) + \alpha \mathbf{M} \times \frac{d\mathbf{M}}{dt} \quad (3.31)$$

where J is exchange constant between the conducting electrons and magnetization, and M_s is saturation magnetization.

3.5 Numerical experiments

3.5.1 Multi-layered structure

We consider a multi-layered spin valve system depicted in figure 3.7. The system consists of two ferromagnetic layers separated by a 5 nm long nonmagnetic spacer, the lengths of two ferromagnetic layers are 10 nm and 5 nm respectively, two 4nm long nonmagnetic leads are set at the ends of the cuboid valve. Since the magnetization configurations in magnetic volumes are homogeneous, the lateral dimensions of the system have no impact on the solutions, we set it 1nm. For the magnetic layers, we choose typical parameters of Heusler alloy, $D_0=1\times 10^{-3}$ m²/s, $\beta = \beta'=0.8$, $\lambda_{sf} = 8$ nm and $\lambda_J = 1$ nm. $D_0=5\times 10^{-3}$ m²/s for both spacer and leads, $\lambda_{sf} = 100$ nm for spacer and $\lambda_{sf} = 11.6$ nm for two leads which are simulated to be infinite [50], and λ_J is unnecessary for nonmagnetic layers.

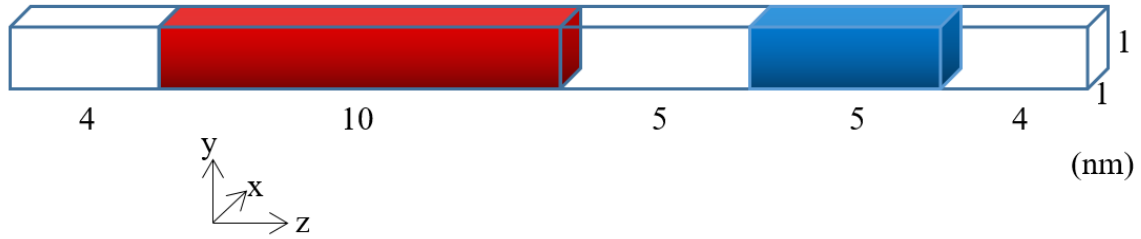


Figure 3.7: Multi-layer spin valve

In the micromagnetic simulation, the 10nm long magnetic layer is thought of as the pinned layer and is homogeneously magnetized into x direction, the other magnetic layer is free layer and it is homogeneously magnetized into y direction. An electric current whose current density is set to be $J_e = 10^{12}$ A/m² flows through the system in z direction. The reaction time of

the magnetization is two orders of magnitude greater than the time needed for the spin accumulation to reach the equilibrium [45], hence we solve the spin accumulation at each node every timestep $\tau = 0.5\text{fs}$ with the magnetization being fixed in the process.

Table 3.1: Timing statistics – solution in multi-layered structure by node-based method

Timing statistics for multi-layered structure		Node-based method			
		No preconditioner	ILU(0)	ILUT	Inverse matrix
Preprocess	Get geometry and initialize (s)	17.636	17.177	16.94	16.884
	Update magnetization (s)	0.001	0.002	0.001	0.001
	Create matrix (s)	3.237	3.298	3.176	3.285
Total preprocessing time (s)		20.874	20.477	20.117	20.17
Compute (10 time-steps)	Fill matrix (s)	0.639	0.631	0.615	0.634
	Compute preconditioner matrix (s)		0.162	0.2	0.543
	Update right-hand side(RHS) (s)	0.003	0.001	0.002	0.001
	RHS by preconditioner (s)		0.027	0.025	0.273
	GMRES solver (s)	19.664	8.538	7.833	
	Total iterations in GMRES	2042	288	156	
Total computation time (s)		20.306	9.359	8.675	1.451
Total time (s)		41.18	29.836	28.792	21.621

Table 3.2: Timing statistics – solution in multi-layered structure by element-based method

Timing statistics for multi-layered structure		Element-based method			
		No preconditioner	ILU(0)	ILUT	Inverse matrix
Preprocess	Get geometry and initialize (s)	11.526	11.466	11.429	11.399
	Update magnetization (s)	0	0	0	0
	Create matrix (s)	2.271	2.295	2.266	2.251
Total preprocessing time (s)		13.797	13.761	13.695	13.65
Compute (10 time-steps)	Fill matrix (s)	0.466	0.451	0.45	0.451
	Compute preconditioner matrix (s)		0.093	0.569	0.475
	Update right-hand side(RHS) (s)	0.068	0.067	0.067	0.066
	RHS by preconditioner (s)		0.022	0.035	0.219
	GMRES solver (s)	11.489	8.177	7.516	
	Total iterations in GMRES	1133	311	86	
Total computation time (s)		12.023	8.81	8.637	1.211
Total time (s)		25.82	22.571	22.333	14.861

First, we compare the solutions of the two computational methods in figure 3.8 and three components of the spin accumulation at $t = 5\text{fs}$ are solved for. The blue and red curves represent the Galerkin method weak solution and the node-based method solution, respectively. We can find they mostly overlap each other and the differences between them in the spacer and leads are small enough to be accepted. Therefore, the both computational methods introduced in section 3.4 can solve the spin diffusion model well.

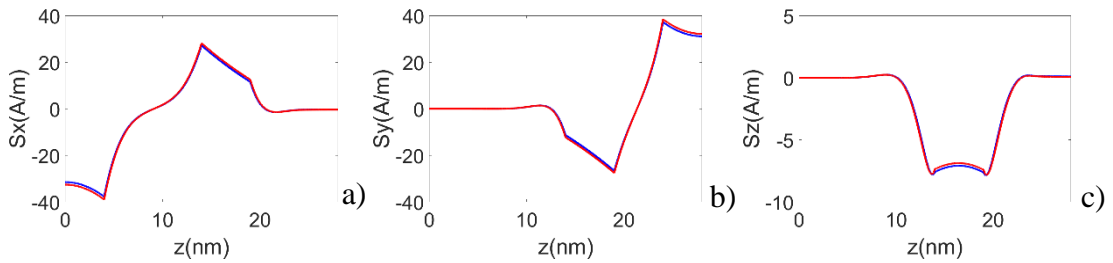


Figure 3.8: Comparison between node-based method solution (red) and Galerkin method weak solution (blue), a), b) and c) are x, y, z component spin accumulation respectively along z axis when $t = 5\text{fs}$.

In addition, timing statistics of node-based method and element-based method are presented in table 3.1 and 3.2 respectively. They include the total time used to achieve the solution after 10 time-steps and the partial time for some important steps, note that the model mesh has about 7000 nodes. We can find that the preconditioners effectively decrease the total iterations number in GMRES solver for both discretization approaches, improving the computational performance.

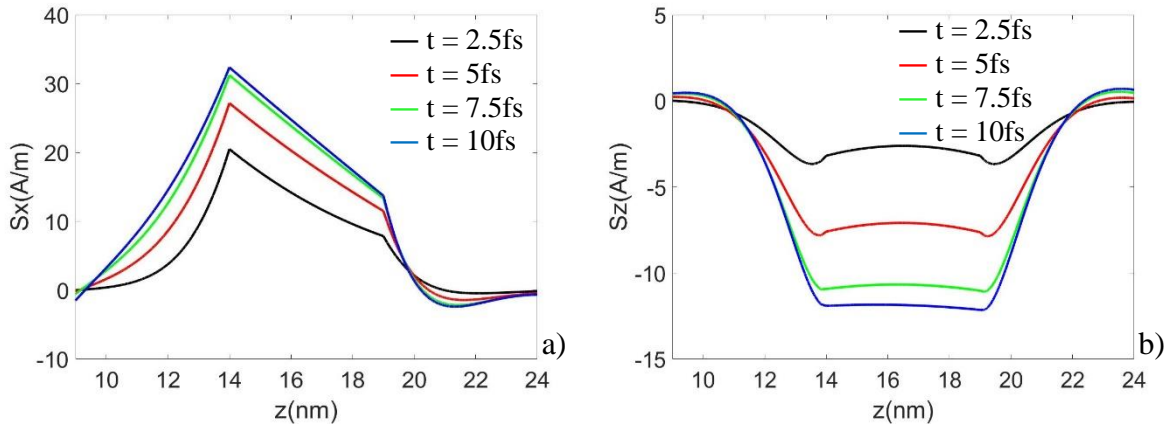


Figure 3.9: a) Variation of the x component of the spin accumulation in the valve along the z axis from 9 to 24 nm, four successive points in time are chosen. b) Variation of the z component of the spin accumulation in the valve along the z axis from 9 to 24 nm, four successive points in time are chosen.

The x and z components of the spin accumulation in the free layer, spacer and the right half of the pinned layer at $t = 2.5, 5, 7.5, 10$ fs are shown in figure 3.9 a) and b), respectively. The x component of the spin accumulation is generated at the interface ($z=14$ nm) between the pinned layer that is magnetized in x direction and the spacer and it then diffuses rapidly from the source, resulting in the build-up of the spin accumulation on the both sides.

However, the spin accumulation tapers off with increasing distance from the interface as discussed in section 3.2, until reaching the interface between the free layer and the spacer where a sharp downward turning occurs. This decrease in spin polarization is due to the strong interaction between the spin accumulation and the y -oriented magnetization in free layer. The interaction is represented by the term $(\mathbf{s} \times \mathbf{m})/\lambda_f^2$ in equation (3.6), which is also the reason for the generation of the z component spin accumulation, which accumulates in both pinned and free layers and then diffuses as depicted in figure 3.9 b).

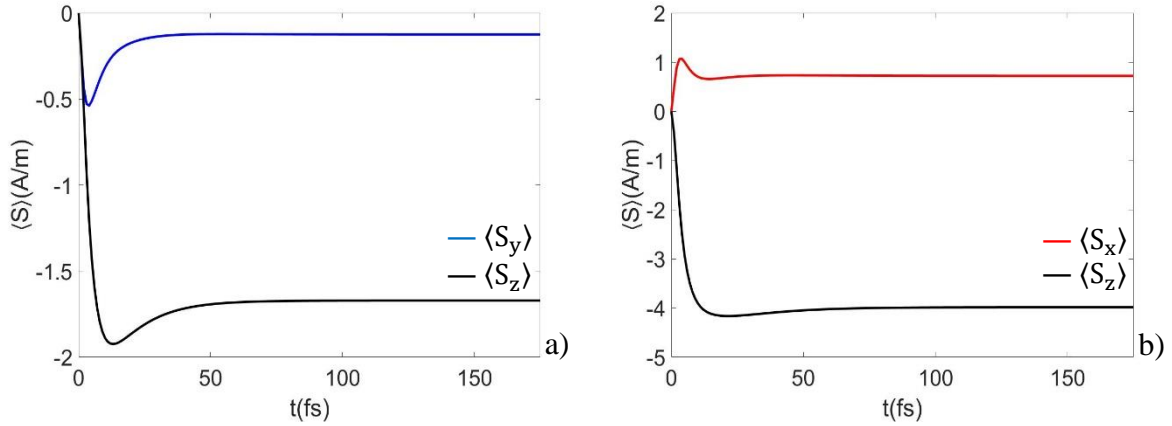


Figure 3.10: a) Evolution of spatially averaged y and z component of the spin accumulation in the pinned layer. b) Evolution of spatially averaged x and z component of the spin accumulation in the free layer.

In order to further study the evolution of the spin accumulation in longer period, we compute the spatially averaged spin accumulation of the discrete components: average S_y and S_z in pinned layer, average S_x and S_z in the free layer, at every single timestep from 0 to 175 fs (figure 3.10). We can find that the spin accumulation builds up rapidly before peaking in about 20 fs, the following relaxation process takes about 120 more femtoseconds to reach equilibrium. The spin accumulation in equilibrium state can be obtained by solving the equations (3.12) or (3.26) when $\partial \mathbf{s} / \partial t = 0$, the solutions are depicted in figure 3.11.

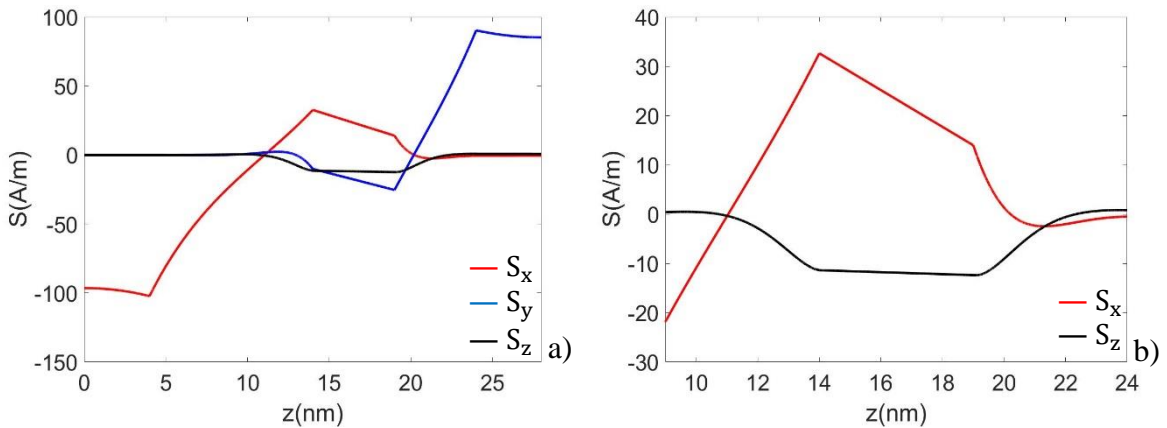


Figure 3.11: a) Spin accumulation in equilibrium along the z axis, components in all directions are shown. b) Zooming in of a) from 9 to 24 nm, x and z components of the spin accumulation are shown.

3.5.2 Néel domain wall

The second model is a thin bar with dimensions $600 \times 100 \times 1$ nm. The material parameters are $D_0 = 1 \times 10^{-3}$ m²/s, $\beta = \beta' = 0.8$, $\lambda_{sf} = 8$ nm and $\lambda_J = 4$ nm. A Néel domain wall is initially set in the middle of the thin bar, the magnetization rotates in the plane from the left to the right (figure 3.12), the spin accumulation at equilibrium is solved, $\partial \mathbf{s} / \partial t = 0$ with homogeneous current density 2.5×10^{11} A/m² pointing in positive x direction in the entire system. Since the magnetization varies only in the x - y plane, two-dimensional vector plots are enough to display the configurations of the magnetization and the spin accumulation in the system (figure 3.13).

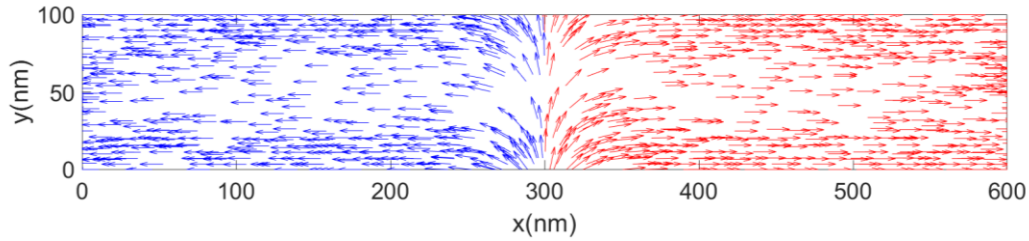


Figure 3.12: The Néel domain wall in the $600 \times 100 \times 1$ nm bar, the magnetization vectors whose x component is positive are colored red, otherwise blue.

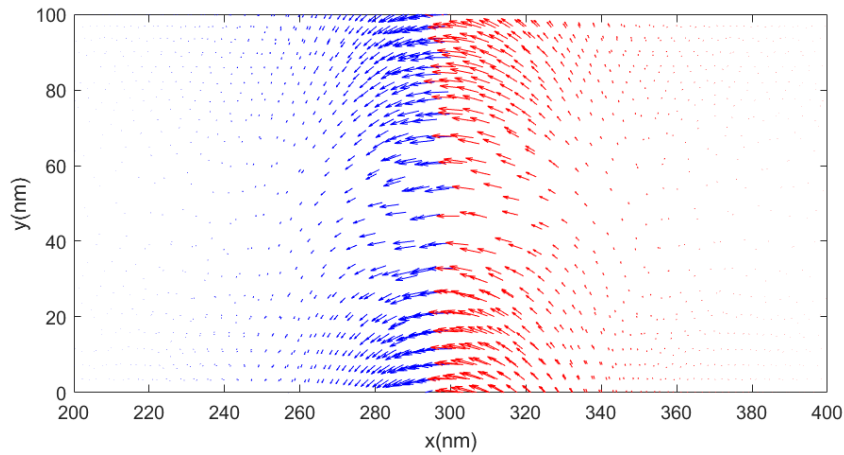


Figure 3.13: Spin accumulation vectors in the bar from $x = 200$ to 400 nm, the vectors whose y component is positive are colored red, otherwise blue.

Similarly, timing statistics for node and element based methods are presented in table 3.3 and 3.4 respectively. In Néel domain wall case, the preconditioners also speed up the convergence of the solution, i.e. computation by GMRES solver.

Table 3.3: Timing statistics – solution in Néel wall case by node-based method

Timing statistics for Néel wall		Node-based method			
		No preconditioner	ILU(0)	ILUT	Inverse matrix
Preprocess	Get geometry and initialize (s)	10.61	10.439	10.394	10.385
	Update magnetization (s)	0.001	0.001	0.001	0.001
	Create matrix (s)	2.043	2.198	2.062	2.196
Total preprocessing time (s)		12.654	12.638	12.457	12.582
Compute (1 time-step)	Fill matrix (s)	0.323	0.32	0.32	0.325
	Compute preconditioner matrix (s)		0.074	0.595	0.311
	Update right-hand side(RHS) (s)	0	0	0	0
	RHS by preconditioner (s)		0.004	0.005	0.016
	GMRES solver (s)	0.734	0.704	0.683	
	Total iterations in GMRES	49	10	4	
Total computation time (s)		1.057	1.102	1.603	0.652
Total time (s)		13.711	13.74	14.06	13.234

Table 3.4: Timing statistics – solution in Néel wall case by element-based method

Timing statistics for Néel wall		Element-based method			
		No preconditioner	ILU(0)	ILUT	Inverse matrix
Preprocess	Get geometry and initialize (s)	6.063	6.065	5.952	6.034
	Update magnetization (s)	0	0	0	0
	Create matrix (s)	1.598	1.583	1.548	1.566
Total preprocessing time (s)		7.661	7.648	7.5	7.6
Compute (1 time-step)	Fill matrix (s)	0.412	0.398	0.39	0.396
	Compute preconditioner matrix (s)		0.069	0.648	0.309
	Update right-hand side(RHS) (s)	0.006	0.007	0.006	0.006
	RHS by preconditioner (s)		0.004	0.005	0.015
	GMRES solver (s)	0.922	0.684	0.669	
	Total iterations in GMRES	106	12	4	
Total computation time (s)		1.34	1.162	1.718	0.726
Total time (s)		9.001	8.81	9.218	8.326

The spin transfer torque, $\mathbf{m} \times \mathbf{s}$ can be calculated directly using the spin accumulation solved above. The comparison with the spin transfer torque calculated by Zhang & Li model (equation 3.5) is depicted below:

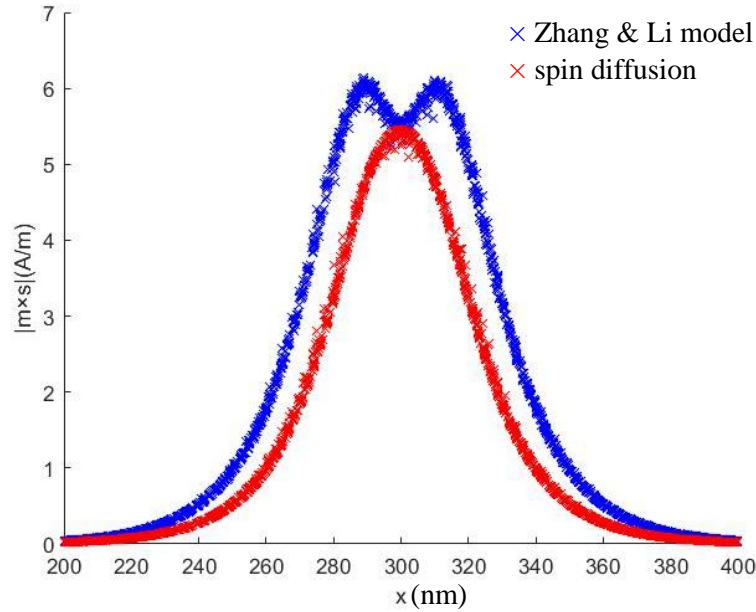


Figure 3.14: Comparison between the magnitude of the spin transfer torque $|\mathbf{m} \times \mathbf{s}|$ calculated by Zhang & Li model and spin diffusion model.

We can find that the spin transfer torques calculated by these two models always have difference, which results from the omission of the gradient of the spin accumulation in Zhang & Li model. However, it is shown in the spin diffusion model that the spin accumulation in the system is not a constant vector.

3.5.3 Magnetization dynamics with STT effect

Consider an MRAM structure (figure 3.15) which is equally divided into five 2-nm-tall layers, the cross section is an ellipse whose long and short axis are 4 and 3 nm respectively.

The blue layer is magnetized in the positive z direction as pinned layer, and the magnetization in the red layer (free layer) is initially aligned to the pinned layer.

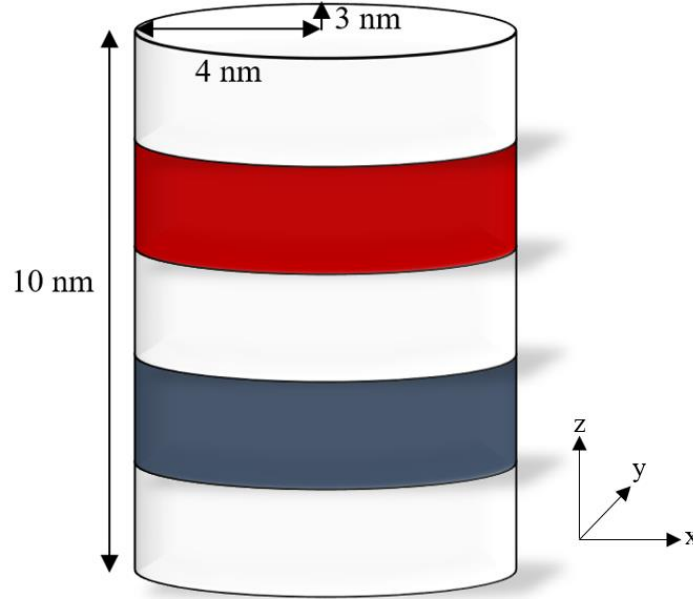


Figure 3.15: MRAM – stacked-layer structure

The magnetic layers' material parameters are set as $D_0 = 1 \times 10^{-3} \text{ m}^2/\text{s}$, $\beta = 0.9$, $\beta' = 0.8$, $\lambda_{sf} = 10 \text{ nm}$ and $\lambda_J = 2 \text{ nm}$, in addition, $K = 13600000 \text{ erg}/\text{cm}^3$, saturation magnetization $M_s = 1432 \text{ emu}/\text{cm}^3$, $A = 1 \times 10^{-6} \text{ erg}/\text{cm}$, and $\alpha = 0.008$. As for the nonmagnetic layers, $D_0 = 5 \times 10^{-3} \text{ m}^2/\text{s}$, $\beta = 0.9$, $\beta' = 0.8$, $\lambda_{sf} = 35 \text{ nm}$ for the leads and $\lambda_{sf} = 100 \text{ nm}$ for the spacer. The magnetization in the free layer is flipped by the spin-polarized electric current whose density is $3 \times 10^{11} \text{ A}/\text{m}^2$ and its dynamics is solved by the FastMag with the maximum timestep = 2 ps. At each time-step of the LLG solution, we assume the spin accumulation to be at equilibrium. The evolution of the magnetization in the free layer is depicted in figure 3.16:

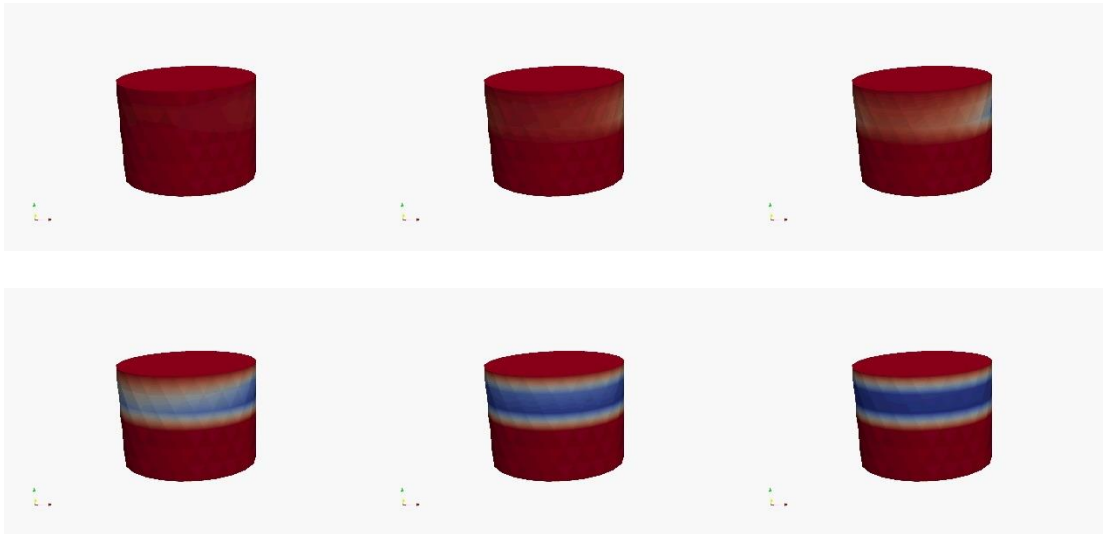


Figure 3.16: Evolution of the magnetization in the free layer, from left to right, top to bottom

the blue and red colors respectively represent the negative and positive z component magnetization, and only magnetic layers and spacer are shown in the figure.

Chapter 4

Conclusion

In this work, we introduced two computational methods and demonstrated their good performance in solving spin diffusion equation in finite element model. The node-based method is straightforward and intuitive, and does not need interpolation of variables, it can be applied in most of the magnetic models except the one whose interface geometry is complex, while the Galerkin method which solves weak formulation based on each element is more general. As for computational performance, the preconditioners can effectively accelerate convergence of the solutions. Then we exploited the spin diffusion model to study the spin dynamics in nanomagnetic structures. The evolution of the spin accumulation in a multi-layer magnetic structure and the spin accumulation under equilibrium state are solved and discussed. We also solved for spin accumulation generated by a Néel wall, the corresponding spin transfer torque was calculated and compared with that calculated by Zhang & Li model. Finally, we coupled the micromagnetic LLG equation with the spin diffusion equation to study the impact of the spin transfer effect on magnetization dynamics.

The spin diffusion model is powerful and comprehensive, different from other models for spin transfer effect, it can solve both dynamic and steady spin accumulation. In addition, the model is not limited to multi-layer magnetic structures and domain walls, it can be applied

in more situations than Slonczewski and Zhang & Li model. Coupled with the spin diffusion model, micromagnetics can deal with more problems. The micromagnetic simulation is the cheapest and the most efficient tool for the design of magnetic devices, its development is essential to scientific researches and industrial applications.

Bibliography

- [1] Johnson, Mark, and Robert H. Silsbee. "Interfacial charge-spin coupling: Injection and detection of spin magnetization in metals." *Physical Review Letters* 55, no. 17 (1985): 1790.
- [2] Baibich, Mario Norberto, Jean Marc Broto, Albert Fert, F. Nguyen Van Dau, Frédéric Petroff, P. Etienne, G. Creuzet, A. Friederich, and J. Chazelas. "Giant magnetoresistance of (001) Fe/(001) Cr magnetic superlattices." *Physical review letters* 61, no. 21 (1988): 2472.
- [3] Binasch, Grünberg, Peter Grünberg, F. Saurenbach, and W. Zinn. "Enhanced magnetoresistance in layered magnetic structures with antiferromagnetic interlayer exchange." *Physical review B* 39, no. 7 (1989): 4828.
- [4] Wolf, S. A., D. D. Awschalom, R. A. Buhrman, J. M. Daughton, S. Von Molnar, M. L. Roukes, A. Yu Chtchelkanova, and D. M. Treger. "Spintronics: a spin-based electronics vision for the future." *Science* 294, no. 5546 (2001): 1488-1495.
- [5] Zhu, Jian-Gang. "Magnetoresistive random access memory: The path to competitiveness and scalability." *Proceedings of the IEEE* 96, no. 11 (2008): 1786-1798.
- [6] Brown, William Fuller. *Micromagnetics*. No. 18. Interscience Publishers, 1963.
- [7] Landau, L.D. and Lifshitz, E.M. "On the Theory of the Dispersion of Magnetic Permeability in Ferromagnetic Bodies." *Phys. Z. Sowjetunion*, no. 8 (1935): 153-164.
- [8] Gilbert, Thomas L. "A phenomenological theory of damping in ferromagnetic materials." *IEEE Transactions on Magnetics* 40, no. 6 (2004): 3443-3449.
- [9] Berkov, Dmitri V. "Magnetization Dynamics Including Thermal Fluctuations: Basic Phenomenology, Fast Remagnetization Processes and Transitions Over High-energy Barriers." *Handbook of Magnetism and Advanced Magnetic Materials*(2007).
- [10] Cullity, Bernard Dennis, and Chad D. Graham. *Introduction to magnetic materials*. John Wiley & Sons, 2011.

- [11] Rikvold, Per Arne, H. Tomita, S. Miyashita, and Scott W. Sides. "Metastable lifetimes in a kinetic Ising model: dependence on field and system size." *Physical Review E* 49, no. 6 (1994): 5080.
- [12] Scholz, Werner, Thomas Schrefl, and Josef Fidler. "Micromagnetic simulation of thermally activated switching in fine particles." *Journal of Magnetism and Magnetic Materials* 233, no. 3 (2001): 296-304.
- [13] Zhu, B., Chester CH Lo, S. J. Lee, and David C. Jiles. "Micromagnetic modeling of the effects of stress on magnetic properties." *Journal of Applied Physics* 89, no. 11 (2001): 7009-7011.
- [14] Chikazumi, Sōshin. *Physics of magnetism*. Wiley, 1964.
- [15] Moskowitz, R., and E. Della Torre. "Theoretical aspects of demagnetization tensors." *IEEE Transactions on Magnetics* 2, no. 4 (1966): 739-744.
- [16] Coey, John MD. *Magnetism and magnetic materials*. Cambridge University Press, 2010.
- [17] van der Laan, Gerrit. "Microscopic origin of magnetocrystalline anisotropy in transition metal thin films." *Journal of Physics: Condensed Matter* 10, no. 14 (1998): 3239.
- [18] Daalderop, G. H. O., P. J. Kelly, and M. F. H. Schuurmans. "Magnetocrystalline anisotropy and orbital moments in transition-metal compounds." *Physical Review B* 44, no. 21 (1991): 12054.
- [19] Tehrani, Said, J. M. Slaughter, E. Chen, M. Durlam, J. Shi, and M. DeHerren. "Progress and outlook for MRAM technology." *IEEE Transactions on Magnetics* 35, no. 5 (1999): 2814-2819.
- [20] Asti, G., and F. Bolzoni. "Theory of first order magnetization processes: Uniaxial anisotropy." *Journal of Magnetism and Magnetic Materials* 20, no. 1 (1980): 29-43.
- [21] Asti, G., F. Bolzoni, F. Licci, and M. Canali. "First order magnetization processes in uniaxial crystals:(Zn, Co) 2 BaFe 16 O 27." *IEEE Transactions on Magnetics* 14, no. 5 (1978): 883-885.
- [22] Bean, C. P., J. D. Livingston, and D. S. Rodbell. "The anisotropy of very small cobalt particles." *J. phys. radium* 20, no. 2-3 (1959): 298-302.
- [23] Weiss, Pierre. "L'hypothèse du champ moléculaire et la propriété ferromagnétique." *J. Phys. Theor. Appl.* 6, no. 1 (1907): 661-690.

- [24] Pauli, Wolfgang. "Über den Zusammenhang des Abschlusses der Elektronengruppen im Atom mit der Komplexstruktur der Spektren." *Zeitschrift für Physik* 31, no. 1 (1925): 765-783.
- [25] Heisenberg, Werner. "Zur theorie des ferromagnetismus." *Zeitschrift für Physik* 49, no. 9-10 (1928): 619-636.
- [26] Bloch, F. "On the theory of the exchange problem and the remanence phenomenon of ferromagnets." *Z. Phys* 74 (1932): 295.
- [27] Néel, Louis. "Remarques sur la théorie des propriétés magnétiques des couches minces et des grains fins." *J. phys. radium* 17, no. 3 (1956): 250-255.
- [28] Yakushiji, Kay, Shinji Yuasa, Taro Nagahama, Akio Fukushima, Hitoshi Kubota, Toshikazu Katayama, and Koji Ando. "Spin-transfer switching and thermal stability in an FePt/Au/FePt nanopillar prepared by alternate monatomic layer deposition." *Applied physics express* 1, no. 4 (2008): 041302.
- [29] Bhatti, Sabpreet, Rachid Sbiaa, Atsufumi Hirohata, Hideo Ohno, Shunsuke Fukami, and S. N. Piramanayagam. "Spintronics based random access memory: a review." *Materials Today* (2017).
- [30] Slonczewski, John C. "Current-driven excitation of magnetic multilayers." *Journal of Magnetism and Magnetic Materials* 159, no. 1-2 (1996): L1-L7.
- [31] Berger, Luc. "Emission of spin waves by a magnetic multilayer traversed by a current." *Physical Review B* 54, no. 13 (1996): 9353.
- [32] Slonczewski, J. C. "Currents and torques in metallic magnetic multilayers." *Journal of Magnetism and Magnetic Materials* 247, no. 3 (2002): 324-338.
- [33] Zhang, S., and Z. Li. "Roles of nonequilibrium conduction electrons on the magnetization dynamics of ferromagnets." *Physical Review Letters* 93, no. 12 (2004): 127204.
- [34] Valet, T., and A. Fert. "Theory of the perpendicular magnetoresistance in magnetic multilayers." *Physical Review B* 48, no. 10 (1993): 7099.
- [35] Mott, Nevill Francis. "The electrical conductivity of transition metals." *Proc. R. Soc. Lond. A* 153, no. 880 (1936): 699-717.
- [36] Hubbard, J. "Exchange splitting in ferromagnetic nickel." *Proceedings of the Physical Society* 84, no. 4 (1964): 455.
- [37] Levy, Peter M., Shufeng Zhang, and Albert Fert. "Electrical conductivity of magnetic multilayered structures." *Physical review letters* 65, no. 13 (1990): 1643.

- [38] Johnson, Mark. "Spin accumulation in gold films." *Physical review letters* 70, no. 14 (1993): 2142.
- [39] Zhang, Shufeng. "Spin Hall effect in the presence of spin diffusion." *Physical review letters* 85, no. 2 (2000): 393.
- [40] Žutić, Igor, Jaroslav Fabian, and S. Das Sarma. "Spintronics: Fundamentals and applications." *Reviews of modern physics* 76, no. 2 (2004): 323.
- [41] Bloch, Felix. "Nuclear induction." *Physical review* 70, no. 7-8 (1946): 460.
- [42] Torrey, Henry C. "Bloch equations with diffusion terms." *Physical review* 104, no. 3 (1956): 563.
- [43] Kaplan, Jerome I. "Application of the diffusion-modified Bloch equation to electron spin resonance in ordinary and ferromagnetic metals." *Physical Review* 115, no. 3 (1959): 575.
- [44] Gurney, Bruce A., Virgil S. Speriosu, Jean-Pierre Nozieres, Harry Lefakis, Dennis R. Wilhoit, and Omar U. Need. "Direct measurement of spin-dependent conduction-electron mean free paths in ferromagnetic metals." *Physical review letters* 71, no. 24 (1993): 4023.
- [45] Zhang, Shufeng, P. M. Levy, and A. Fert. "Mechanisms of spin-polarized current-driven magnetization switching." *Physical review letters* 88, no. 23 (2002): 236601.
- [46] Lubarda, Marko V. *Micromagnetic Modeling and Analysis for Memory and Processing Applications*. University of California, San Diego, 2012.
- [47] García-Cervera, Carlos J., and Xiao-Ping Wang. "Spin-polarized currents in ferromagnetic multilayers." *Journal of computational physics* 224, no. 2 (2007): 699-711.
- [48] Abert, Claas, Michele Ruggeri, Florian Bruckner, Christoph Vogler, Gino Hrkac, Dirk Praetorius, and Dieter Suess. "A three-dimensional spin-diffusion model for micromagnetics." *Scientific reports* 5 (2015): 14855.
- [49] Jin, Jian-Ming. *The finite element method in electromagnetics, 2nd edition*. John Wiley & Sons, 2015.
- [50] Abert, Claas, Hossein Sepehri-Amin, Florian Bruckner, Christoph Vogler, Masamitsu Hayashi, and Dieter Suess. "Field-and damping-like spin-transfer torque in magnetic multilayers." *arXiv preprint arXiv:1612.00194* (2016).